JOURNAL OF PETROLOGY | VOLUME 51 | NUMBERS 1 & 2 | PAGES 55–80 | 2010 | doi:10.1093/petrology/egp059

The Role of Pyroxenites in Formation of Shear Instabilities in the Mantle: Evidence from an Ultramafic Ultramylonite, Twin Sisters Massif, Washington

VIRGINIA G. TOY[1]*, JULIE NEWMAN[2], WILLIAM LAMB[2] AND BASIL TIKOFF[3]

[1]DEPARTMENT OF GEOLOGY, UNIVERSITY OF OTAGO, PO BOX 56, DUNEDIN 9054, NEW ZEALAND

[2]DEPARTMENT OF GEOLOGY AND GEOPHYSICS, TEXAS A&M UNIVERSITY, COLLEGE STATION, TX 77843-3115, USA

[3]DEPARTMENT OF GEOLOGY AND GEOPHYSICS, UNIVERSITY OF WISCONSIN–MADISON, 1215 W DAYTON ST., MADISON, WI 53706, USA

RECEIVED JANUARY 2, 2009; ACCEPTED AUGUST 11, 2009
ADVANCE ACCESS PUBLICATION NOVEMBER 4, 2009

In the Twin Sisters ultramafic massif, NW Washington, an ~0·5 cm thick, isolated ultramafic ultramylonitic shear zone displaces orthopyroxenite and clinopyroxenite dikes, by a minimum of 21 cm. The shear zone exists only adjacent to the orthopyroxenite and clinopyroxenite dikes, with deformation distributed along strike into the wall-rock less than 10 cm from the dikes in the outcrop face. Microstructurally, the shear zone contains domains of different grain sizes and phase proportions. A marginal domain of almost pure olivine displays a mean grain size of ~30–100 μm and an olivine lattice preferred orientation (LPO) indicating that glide occurred on (010)[100] and (010)[001]. A central domain of mixed olivine, pyroxene and amphibole displays a finer grain size, ranging down to ~5 μm. Aligned grain and phase boundaries and weak olivine and pyroxene LPOs indicate that this zone deformed by a grain-size-sensitive deformation mechanism (e.g. grain boundary sliding accompanied by diffusion creep). Geothermometry indicates that shearing occurred at temperatures in the range 650–750°C. We interpret the formation of this ultramylonitic shear zone as a shear instability caused by the presence of compositional heterogeneity. Localization was promoted by a deformation mechanism switch from dislocation creep to grain-size-sensitive creep as a result of syn-deformational grain-size reduction. Mineral compositions indicate that this grain-size reduction was associated with reaction. The fine grain size was stabilized by the presence of multiple phases, particularly pyroxene, within the central shear zone domain. The shear zone did not propagate beyond the vicinity of the pyroxenite dikes because the fine grain sizes necessary for the deformation mechanism switch to occur could not be maintained in the monophase olivine forming the surrounding dunite.

KEY WORDS: *rheological heterogeneity; strain localization; grain-size reduction; grain-size-sensitive creep; pyroxene (010)-glide*

INTRODUCTION

A major difficulty in quantifying rheology is that most rocks are polymineralic (e.g. Handy, 1990, 1994; Ji & Zhao, 1993; Ji *et al.*, 2004). In an attempt to simplify this problem, the rheology of a given polymineralic rock is often assumed to be controlled primarily by the strength of its weakest major phase (e.g. quartz for the upper crust and olivine for the mantle: Goetze & Evans, 1979; Brace & Kohlstedt, 1980; Kirby, 1983; Ranalli & Murphy, 1987). The modal abundance and the degree of connectivity of the weakest phase are two parameters considered in

*Corresponding author. Telephone: +64 3 479 7506. Fax: +64 3 479 7527. E-mail: virginia.toy@otago.ac.nz

models of polymineralic rock rheology (e.g. Tullis *et al.*, 1991; Handy *et al.*, 1999; Imber *et al.*, 2001). A useful conceptual model built from these experiments and field observations emphasizes the transition from a relatively strong, load-bearing framework (for example, of quartz and feldspar) to an interconnected weak phase (e.g. biotite; Handy, 1990, 1994).

However, the presence of a second mineral phase is sometimes sufficient to cause a non-linear change in rheology, relative to the percentage of the second phase. In polyphase materials reaction can accompany deformation, and reaction-induced grain-size reduction has been reported to promote a transition to grain-size-sensitive creep in a range of natural and experimental studies (e.g. Stünitz & Fitz Gerald, 1993; Fliervoet *et al.*, 1997; Holyoke & Tullis, 2006*a*). For example, H_2O-deficient sub-solidus reactions in peridotite cause strain-softening because of a transition from dislocation to grain-size-sensitive creep mechanisms (e.g. Furusho & Kanagawa, 1999; Newman *et al.*, 1999).

Grain-size reduction by dynamic recrystallization appears unable to cause a permanent transition to grain-size-sensitive creep in monophase materials, as material will coarsen until it is again within the dislocation creep field (de Bresser *et al.*, 1998, 2001). A second phase may inhibit grain growth sufficiently to stabilize grain size within the grain-size-sensitive creep field. Furthermore, as illustrated by Wheeler (1992) and Sundberg & Cooper (2008), polyphase aggregates can be much weaker than their end-members during grain-size-sensitive creep, as a result of chemical interactions between diffusing species.

A second effect of a second mineral phase is to cause stress heterogeneities. Locally high stresses are induced in heterogeneous mantle materials, as documented by Jin *et al.* (1998) in the Balmuccia peridotites or by Tikoff *et al.* (in preparation) in folded pyroxenite dikes in the Twin Sisters peridotites. Shear localization in the lithospheric mantle may therefore depend on the distribution of such heterogeneities (e.g. tabular pyroxenite zones), which cause zones of higher strain rate (Treagus & Sokoutis, 1992).

In this paper we describe the geometry, microstructures, crystallographic fabrics and chemical characteristics of an ultramafic ultramylonite from the Twin Sisters massif, and consider the relationship of the shear zone to the aforementioned concepts.

GEOLOGICAL SETTING

The ultramafic massif forming the Twin Sisters Range is located approximately 6 km east of Mt. Baker, in Whatcom County, NW Washington (Fig. 1a). The massif is composed of largely unserpentinized dunite and harzburgite with chrome spinel, minor clinopyroxene, and rare amphibole (Onyeagoucha, 1978). Fabrics observed throughout the massif, in likely order of formation, are a north–south-striking, near vertical dunite/harzburgite compositional layering; a NNW–SSE-striking, steeply ENE-dipping tectonite fabric with foliation and lineation of elongate spinels (Tikoff *et al.*, in preparation; Fig. 1b); and later cross-cutting NNW–SSE-striking, sub-vertical dunite bands that may represent a melt-transport network (Fig. 1c; Kruckenberg *et al.*, 2008). The compositional layering is cross-cut by folded orthopyroxenite dikes with variable orientations and planar cross-cutting north–south-striking, moderately west-dipping websterite and clinopyroxenite dikes (Fig. 1d and e). The latter are coeval with or postdate formation of the tectonite fabric and dunite bands (melt-transport network?). Finally, these structures are offset by mostly east–west-striking faults with centimetre- to metre-scale displacements.

The arrangement and orientations of dikes and late faults were characterized during detailed mapping of a $\sim$90 m^2 area using laser total station. This area is located at an elevation of $\sim$7000 ft, on the north side of North Twin Sister peak. On the eastern margin of this mapped area, an ultramylonitic shear zone in harzburgite was observed to offset an orthopyroxenite dike and a clinopyroxenite dike that are near orthogonal to the shear zone (Fig. 2b). We will focus on the structural development of this shear zone in the remainder of this paper.

FIELD OBSERVATIONS

The geometry of the shear zone and offset markers was characterized by tracing the outcrop onto a Mylar overlay in the field (Fig. 2a). Representative structural measurements were obtained and oriented samples were cored from the shear zone and host-rock.

In the approximately north–south-striking face where the shear zone crops out, a folded orthopyroxenite dike is offset with apparent top-to-the-north sense on an unserpentinized zone <5 mm thick and <1 m long (Fig. 2a). The shear zone contains a weak foliation parallel to its margins and a weak elongation of porphyroclastic grains trending $\sim$230°. A clinopyroxenite dike with similar orientation to the orthopyroxenite dike (Fig. 2a), located near one end of the shear zone, is offset by <3 cm in the outcrop face; this is significantly less than the orthopyroxenite dike, which is offset 31 cm. Pyroxene grains from both dikes can be traced into the shear zone. The shear zone must terminate at both ends a similar distance (<10 cm) from the offset dikes, as rare orthopyroxene grains in the host dunite are no longer offset across its expected continuation.

The offset orthopyroxenite dike is relatively planar for a distance of $\sim$70 cm in the area adjacent to the shear zone. Further along strike of the dike, away from the shear zone, the orthopyroxenite dike is deformed by centimetre-wavelength, asymmetric, west-verging, open folds around

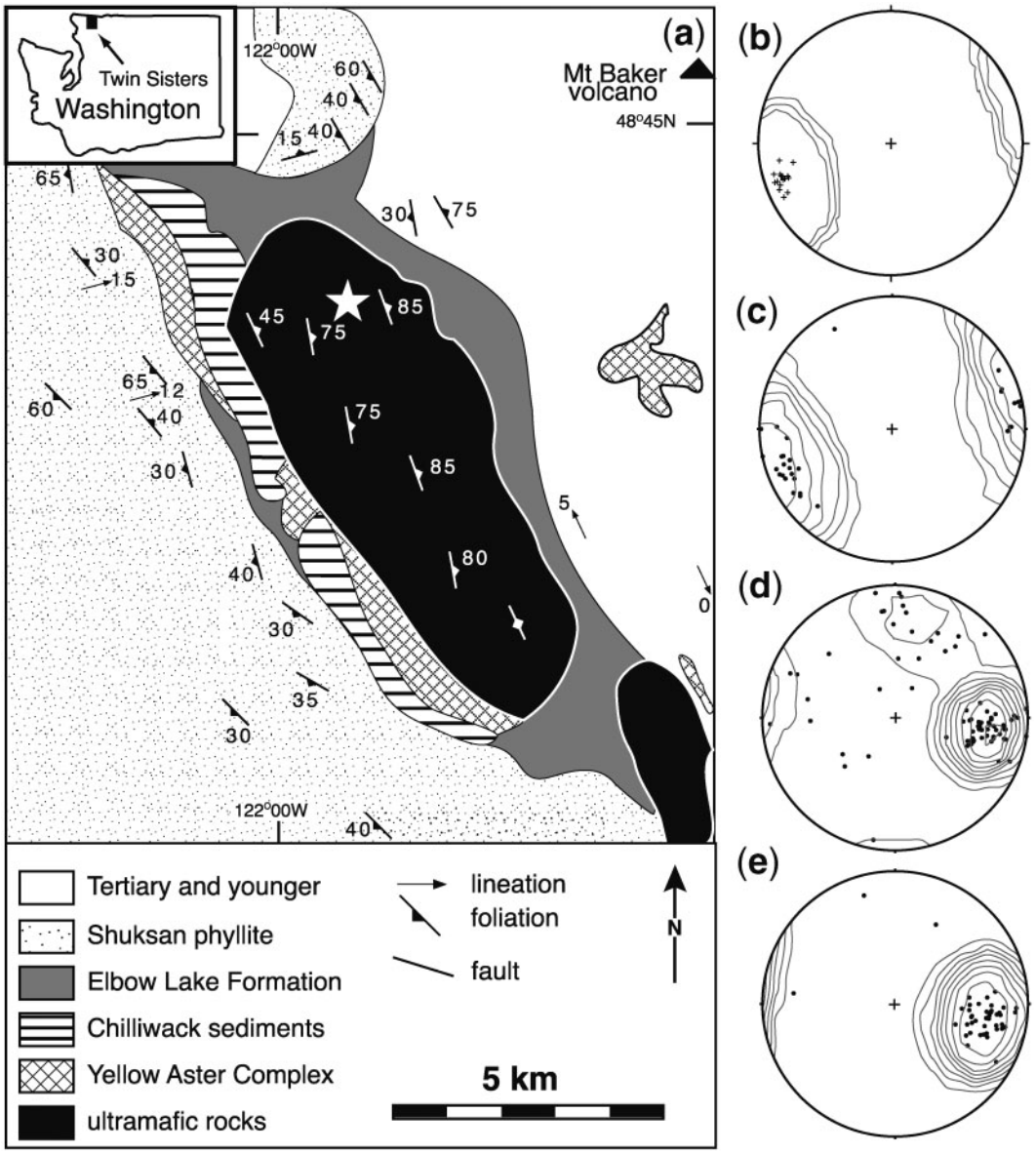

Fig. 1. (a) Regional geological map of the Twin Sisters massif, modified from Ferre *et al.* (2005). Location of shear zone indicated by white star. (b–e) Equal area lower hemisphere stereoplots illustrating orientations of structural fabrics in the massif. Contouring by the Kamb method with contour interval = 2·0. (b) Poles to foliation; entire massif. $N = 19$. (c) Poles to spinel seams, immediate vicinity of shear zone. These seams are parallel to late dunite bands that may represent melt channels. $N = 31$. (d) Poles to orthopyroxenite dikes, immediate vicinity of shear zone. $N = 82$. (e) Poles to clinopyroxenite dikes, immediate vicinity of shear zone. $N = 46$.

a mean hinge line plunging 36° towards 160° in the immediate vicinity of the shear zone (Fig. 2e). The hinge-line orientation varies further along the dike from the shear zone. On the other hand, the fold axial plane is everywhere consistently oriented ~162°/79°E, subparallel to a foliation (oriented approximately 159°/72°NE) defined by grain shape preferred orientation of spinels and orthopyroxene in the host-rock (Fig. 2e). This foliation contains a lineation defined by elongate spinels that pitches moderately to the NW (23°/347°).

PETROLOGICAL AND MICROSTRUCTURAL OBSERVATIONS

We took samples of the shear zone from near where the orthopyroxenite and clinopyroxenite dikes intersect it (samples NC07-16f and NC07-16a, respectively), and a sample of the shear zone between the offset orthopyroxenite dike segments (sample NC07-16c). These samples contain both shear zone and host-rock. We also sampled the

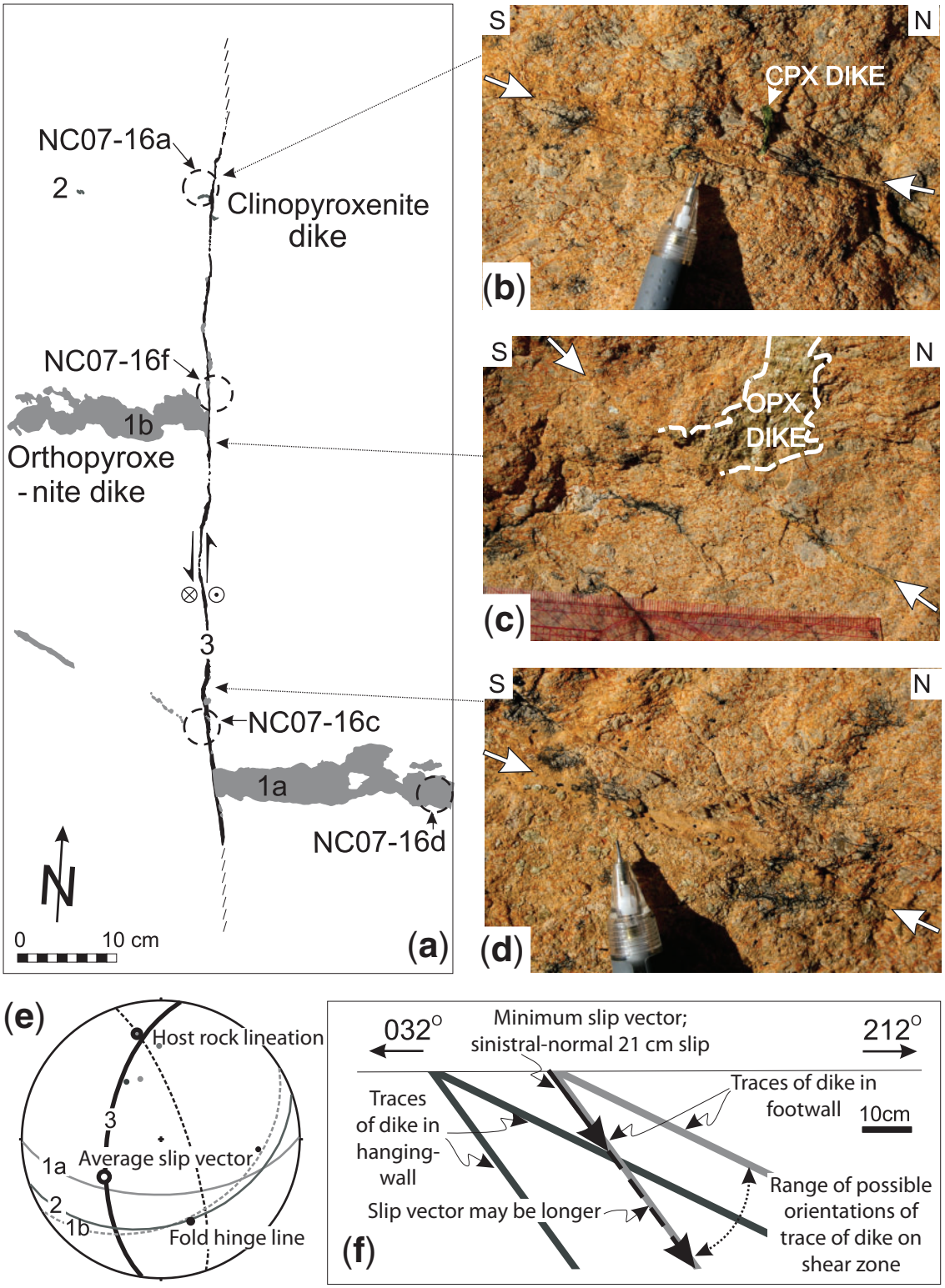

Fig. 2. Shear zone field relationships. (a) Tracing of shear zone and offset markers in outcrop. The outcrop face strikes ~175° and dips moderately to the east. It should be noted that the apparent top-to-the north offset of the orthopyroxenite dike is opposite to the true sense of shear on the zone, and results from juxtaposition of segments of the dike with different orientations in the outcrop face. (b–d) Outcrop photographs of the shear zone and offset markers, at locations along the shear zone indicated by black arrows. In each photograph, the shear zone lies between the white arrows. (e) Equal area lower hemisphere stereoplot illustrating geometric arrangement of shear zone, dikes, and host-rock structures. Great circles represent the offset orthopyroxenite dike (1a and 1b); offset clinopyroxenite dike (2); shear zone (3); and the host-rock foliation (dashed line). These features are also numbered in (a). Unlabelled points are poles to these planes. (f) Sketch looking down on footwall of shear zone, illustrating traces of orthopyroxenite dike and shear zone slip vector. The orientation of the orthopyroxenite dike could range between the measured orientation in the footwall and hanging wall, so the true slip vector length cannot be determined.

Table 1: Estimates of mean recrystallized grain size and modal proportions of various minerals, from BSE images of decorated samples

Location	Olivine			Orthopyroxene			Clinopyroxene			Chrome spinel			Amphibole		
	d*	D*	%†	$\bar{d}$	$\bar{D}$	%	$\bar{d}$	$\bar{D}$	%	$\bar{d}$	$\bar{D}$	%	$\bar{d}$	$\bar{D}$	%
Sample NC07-16f															
(4)	2·6	4·6	60·2	3·2	5·6	39·4				1·1	1·8	0·4			
(4)	4·1	7·3	61·0	2·8	4·8	39·0									
(2)	18·7	32·8	100·0												
Sample NC07-16a															
(5)	9·1	15·9	60·9				38·1	66·6	39·1						
(5)	12·6	22·1	73·0				9·8	17·1	21·2	2·5	4·3	1·2	13·3	23·3	4·6
(2)	24·4	42·8	100·0												
(2)	27·1	57·8	100·0												
(2)	58·9	103·1	100·0												

Locations are shown in Figs 3 and 6.
*Mean grain sizes are in micrometres.
†That is, modal proportion of this phase.

orthopyroxenite dike some distance from the shear zone (sample NC07-16d). The locations of these samples are indicated in Fig. 2a. In the following discussion of these samples we refer to a right-handed reference frame where X_H is parallel to the host-rock lineation, X_{SZ} is parallel to the lineation and shear direction in the shear zone, Z_H is the pole to the host-rock foliation, and Z_{SZ} is the pole to the shear zone boundary.

We first made observations of mineral assemblages, microstructures and phase arrangement in oriented petrographic thin sections cut from the oriented cores. Microstructures were subsequently further characterized using electron microscopic methods.

Phase proportions and grain sizes within the shear zone were determined from backscattered electron (BSE) images obtained using an FEI Quanta 600 FE-SEM at Texas A&M University. Dislocations in olivine and olivine grain boundaries were made more visible in BSE mode using the oxidization-decoration technique described by Kohlstedt (1976). Samples were heated to 900°C for only ~45 min to prevent the decoration from obscuring detail in fine-grained material (see Newman *et al.*, 1999).

Grain-size and phase proportion analyses

BSE images were obtained from X_{SZ}–Z_{SZ} sections from areas of the samples with representative grain-size distributions. Three to five images were obtained from each area at a variety of magnifications, so that most grains had lengths of 1–2 cm in printed images. Grain outlines were manually traced onto Mylar overlays. Phases were false-coloured, and the resulting grain boundary maps were analysed using ImageSXM software from the University of Liverpool to determine grain-size distributions and phase proportions. The reported grain diameter, $\bar{d}$, is the geometric mean of the diameters of circles of equivalent area to each grain within an aggregate. Means are from a minimum of 100 grains. It is common to apply a stereological correction to estimate the three-dimensional grain size from observations in a two-dimensional section (e.g. Exner, 1972). It is questionable whether such methods correctly account for variations in grain dimension when there is a grain shape preferred orientation, as in our samples. Furthermore, there are a wide range of possible correction factors. Hence, we present both $\bar{d}$ and $\bar{D}$, the geometric mean grain size corrected by a factor of 1·75 times, for consistency with the van der Wal *et al.* (1993) paleopiezometric relationship. Estimates of recrystallized grain sizes and phase proportions within various microstructural domains of the shear zone are presented in Table 1 and Fig. 3.

Host-rock

The peridotite outside the shear zone is dunite, with very minor orthopyroxene and clinopyroxene, and trace amphibole. It has a porphyroclastic microstructure with large olivine and pyroxene grains ranging from 0·5–5 mm in diameter and smaller (200–400 μm diameter) olivine grains along the boundaries of larger grains (Figs 3a, b and 4a).

Clinopyroxene and orthopyroxene occur in rare trains at high angles to the shear zone. Some orthopyroxenes have clinopyroxene lamellae and both types of pyroxene contain amphibole inclusions. Sub- to euhedral amphiboles are also observed to partially replace clinopyroxenes,

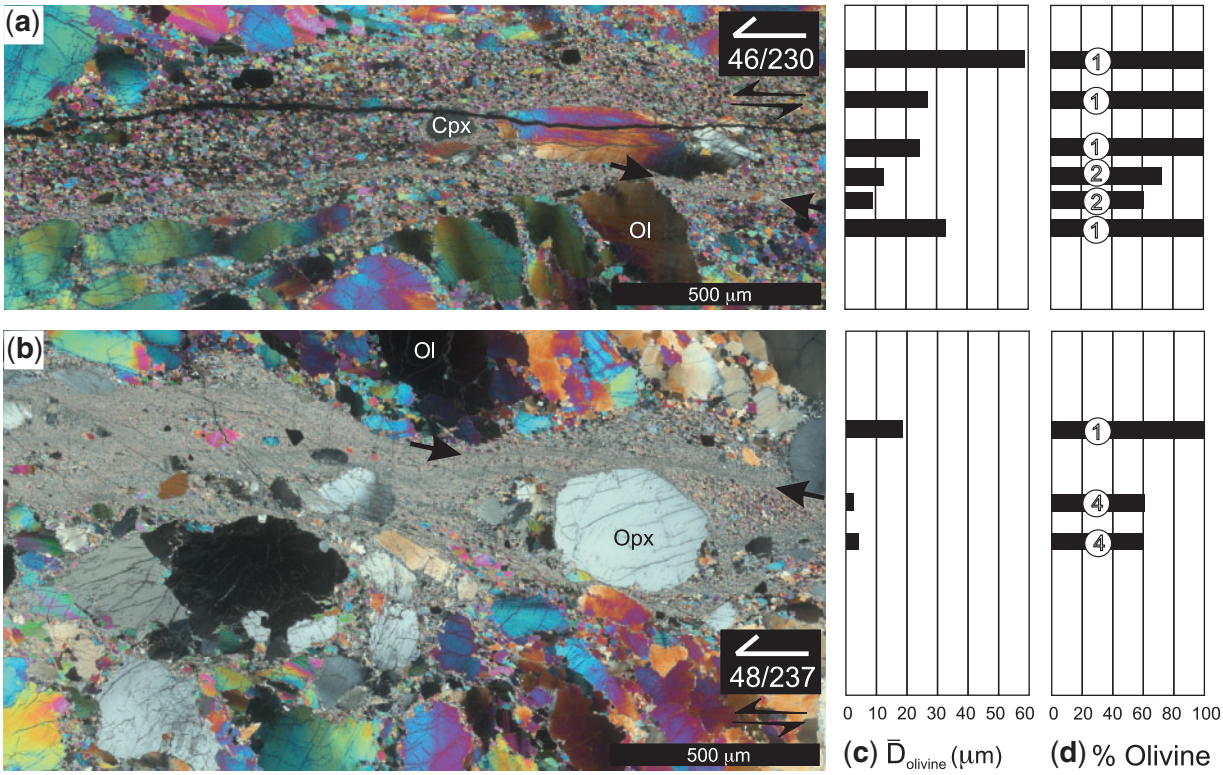

Fig. 3. High-resolution scans of thin sections (a) NC07-16a and (b) NC07-16f. Cross-polarized light. (a) is located near the northern end of the localized shear zone (see Fig. 2). Large host olivine grains surround medium-grained olivine within the shear zone. Very fine-grained material is observed only immediately surrounding clinopyroxene porphyroclasts (such as that labelled 'Cpx'), and in tails from porphyroclasts, such as between the black arrows. (b) is located nearer the centre of the localized shear zone, where the opthopyroxenite dike intersects the zone (see Fig. 2). Most of the sheared material is fine-grained to very fine-grained. The smallest grain sizes occur in layers that anastomose around orthopyroxene porphyroclasts (e.g. between black arrows). Both sections are viewed in an X_{SZ}–Z_{SZ} frame, facing down towards the NW, into the shear zone. Mean grain diameters (c) and phase proportions (d) were determined from backscattered electron images as described in the text. Numbers indicate the type of material, as indicated conceptually in Fig. 6, from which these measurements were made. The locations of the measurements with respect to the images are schematic, as the backscatter images were obtained from different, but parallel slices through these samples.

particularly where they are close to orthopyroxenes (Fig. 5c and d).

The orthopyroxenite dike outside the shear zone (Fig. 4c) is composed of moderately equant, large (0·5–4 mm diameter) grains, with rare smaller (50–100 μm diameter), inequant grains decorating grain boundaries. Large grains are commonly kinked at twin boundaries, and triangular clinopyroxene exsolution lamellae or smaller orthopyroxene grains are found along these kinked twin boundaries. Elsewhere, elongate trains of small orthopyroxene grains have similar orientation to the kinks.

Shear zone

Within the shear zone there are two different compositional domains that also have distinct microstructures (Fig. 6). At the boundary with the host-rock there is an intermediate grain-size domain of almost monophase olivine ranging up to 0·8 mm in thickness. This domain is thickest towards the ends of the shear zone and almost absent near the centre of the zone. The monophase olivine domain encloses a polyphase domain that is composed of fine- to very fine-grained olivine intermixed with pyroxenes, trails of amphibole and fine spinel, with some larger (<5 mm long) pyroxene and spinel porphyroclasts. The polyphase domain is thickest near the centre of the shear zone (a maximum thickness of 0·4 mm is observed in NC07-16f, near the offset orthopyroxenite dike).

Monophase domain

The monophase olivine domain has irregular, inter-tonguing margins with the host. Olivine has $\bar{D}$ ranging from 32 to 100 μm (Fig. 3c). The olivine grains that make up this domain are slightly elongated, with axial ratios up to 1:2 (Fig. 3a). However, undulose extinction is weak to absent, grain boundaries are generally straight to gently curved and 120° triple junctions are common (e.g. Domain A1). Chrome spinel, which forms <5 modal %, is mostly concentrated as large porphyroclasts rather than distributed throughout the olivine aggregates.

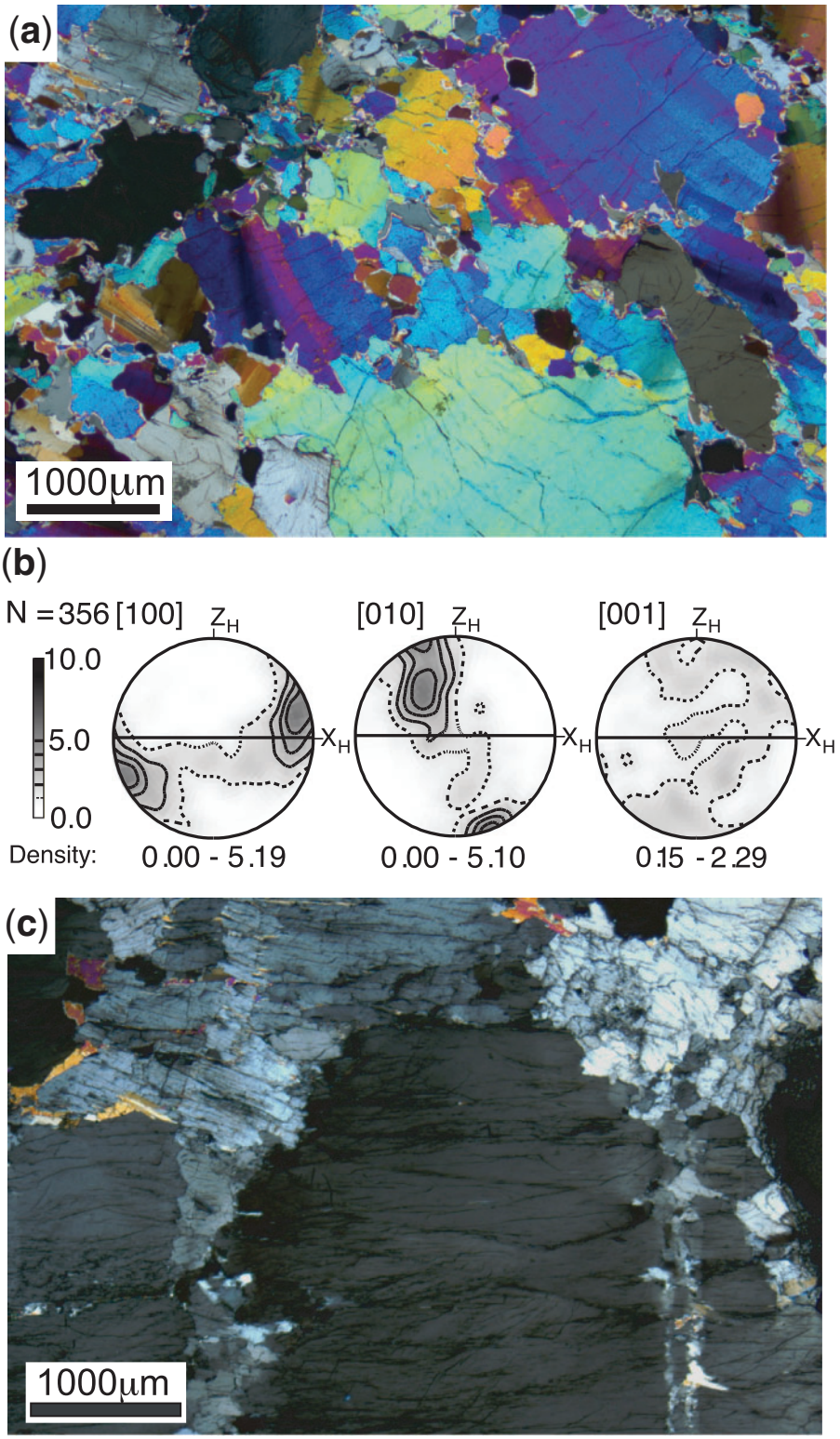

Fig. 4. (a) Photomicrograph illustrating typical host-rock microstructure. Crossed polarizers. (b) Pole figure illustrating host-rock olivine LPO, derived as one point per grain from EBSD map data. Plot is equal area lower hemisphere. Z_H is pole to host-rock foliation; X_H is parallel to the host-rock lineation. Contouring is multiples of uniform density. (c) Photomicrograph illustrating typical microstructure in orthopyroxenite dike outside the shear zone (sample NC07-16d). Crossed polarizers. Noteworthy features are kinking, particularly evident at upper left; clinopyroxene lamellae with higher-order interference colours concentrated at kinks; and trains of smaller grains parallel to kink boundaries.

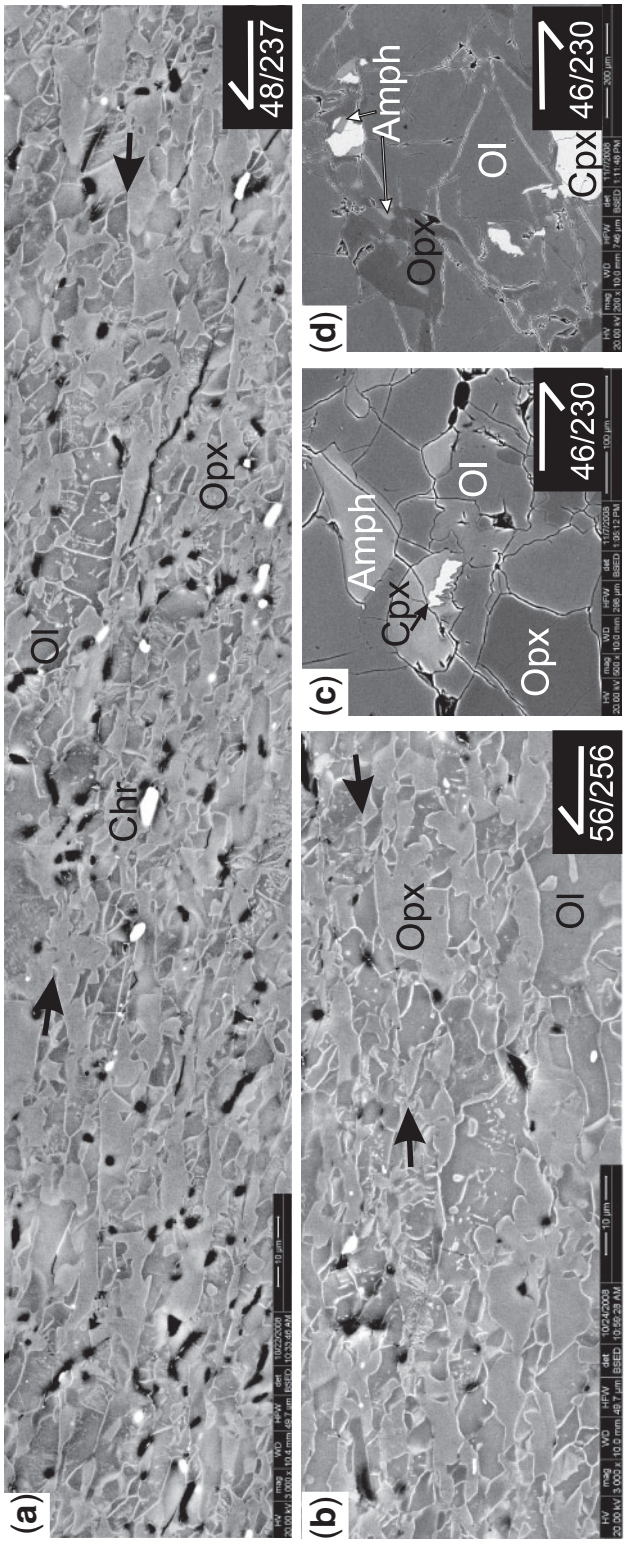

Fig. 5. Backscatter electron images of decorated samples. Grain boundaries and dislocations in olivine appear white in these images. Phases are labelled (Cpx, clinopyroxene; Opx, orthopyroxene; Ol, olivine; Chr, chrome spinel; Amph, amphibole). (a) Finest-grained region in NC07-16f. There is a grain shape preferred orientation and grain and phase boundaries are aligned through multiple grains subparallel to the shear plane (horizontal in this image). (b) A similar fine-grained region in NC07-16c also has well-aligned grain boundaries in finer-grained material towards the upper half of the image. However, with increasing grain size towards the bottom of the image, the grain boundaries become more lobate and randomly oriented. Examples of grain boundaries aligned through multiple grains lie between the black arrows in (a) and (b). (c, d) Textural relationships between clinopyroxene, orthopyroxene, amphibole and olivine in host-rock within NC07-16a. Amphibole replaces clinopyroxene and olivine in (c). In (d), amphibole is seen as inclusions in orthopyroxene (left of image) and as euhedral grains replacing clinopyroxene (top right of image).

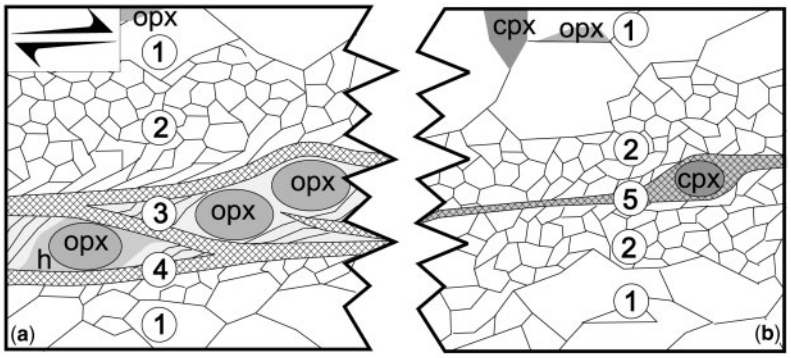

Fig. 6. Schematic illustration of grain-size domains and phase relationships in the shear zone. Host-rock outside the zone (1) is composed of coarse (1–10 mm) olivine grains with rare clinopyroxene (cpx) and orthopyroxene (opx). Inside the shear zone are (2) a margin of coarse, equant olivine; (3) moderately fine-grained mixed orthopyroxene and olivine with an oblique grain shape fabric in porphyroclast pressure shadows; (4) very fine-grained mixed orthopyroxene, olivine and sometimes hornblende in interlinked zones that anastomose about porphyroclasts; (5) fine-grained mixed clinopyroxene, olivine and hornblende in the pressure shadows and tails of clinopyroxene porphyroclasts. Masses of hornblende also sometimes rim orthopyroxene porphyroclasts (h).

However, there are also a few intermediate-grained (~50 μm) spinels.

Polyphase domain

The polyphase domain has comparatively straight margins with the surrounding material. The microstructure changes along the shear zone as the relative abundance of the two types of pyroxene porphyroclasts changes (Fig. 6a vs Fig. 6b). Orthopyroxene porphyroclasts are most common in the central section of the shear zone between the offset orthopyroxenite dike (samples NC07-16c and NC07-16f), whereas clinopyroxene porphyroclasts are mostly found where the clinopyroxenite dike intersects the shear zone (sample NC07-16a). However, these two phases are present in small proportions in all host-rocks examined, and these host grains have also sometimes been incorporated into the shear zone. Some of both types of pyroxene porphyroclasts are rimmed by mantles of moderately fine-grained amphibole, which also becomes progressively intermixed with the other phases with increasing distance from the porphyroclasts (e.g. Fig. 7).

Where significant amounts of orthopyroxene are present, near the centre of the shear zone (samples NC07-16c and NC07-16f; Figs 3b, 6a, 8a, b and 9b, h), a series of very fine-grained mixtures of olivine and orthopyroxene anastomose around orthopyroxene porphyroclasts. The smallest olivine grains were measured in these materials ($\bar{D}$ = 4·6 μm for 60% olivine; Fig. 3c and d). Within these very fine-grained zones, grains are elongate parallel to the shear zone boundaries, and grain and phase boundaries (in the sense of Fitz Gerald & Stünitz, 1993) are commonly aligned through multiple grains (Fig. 5a and b). Grain size varies between thin layers within the shear zone, and with increasing grain size, grain and phase boundaries subparallel to the shear plane become more curved and even interlobate.

Slightly coarser-grained olivine–orthopyroxene aggregates (olivine $\bar{D}$ = 33 μm for 60% olivine; Fig. 3c and d) with axial ratios of the order of 1:2 and oblique grain shape fabrics are found in orthopyroxene porphyroclast pressure shadows. Orthopyroxene porphyroclasts also have tails in which this phase is mixed with increasing proportions of olivine with increasing distance from the orthopyroxene porphyroclasts (Figs 7 and 8b).

Where clinopyroxene porphyroclasts are more common, towards the northern end of the shear zone (sample NC07-16a), fine-grained olivine, clinopyroxene and amphibole are found only within the delta-shaped tails of clinopyroxene porphyroclasts (Figs 6b and 10a, b), in zones strung out between these clinopyroxene porphyroclasts and more rarely in rims around the clinopyroxene prophyroclasts. Olivine $\bar{D}$ in these polyphase domains ranges from 15·9 to 22 μm, with larger grain sizes measured when the ratio of olivine:orthopyroxene is greater (Fig. 3c and d). At the margins of the clinopyroxene porphyroclasts, olivine, clinopyroxene and amphibole have curved grain boundaries, are well mixed, and olivine and amphibole also interfinger into the porphyroclasts (Fig. 10a, top left). Amphibole generally becomes less common with increasing distance from the clinopyroxene porphyroclasts (Fig. 10a).

Electron backscatter diffraction (EBSD)

Methods

Electron backscatter diffraction (EBSD) techniques were used to characterize phase arrangement, microstructural style, and lattice preferred orientations (LPOs) of olivine and pyroxenes in the shear zone, and olivine in the adjacent host-rock. Shear zone layers that exhibit variations in olivine:pyroxene ratios and mean grain size are presented as separate datasets. For these analyses, oriented, polished

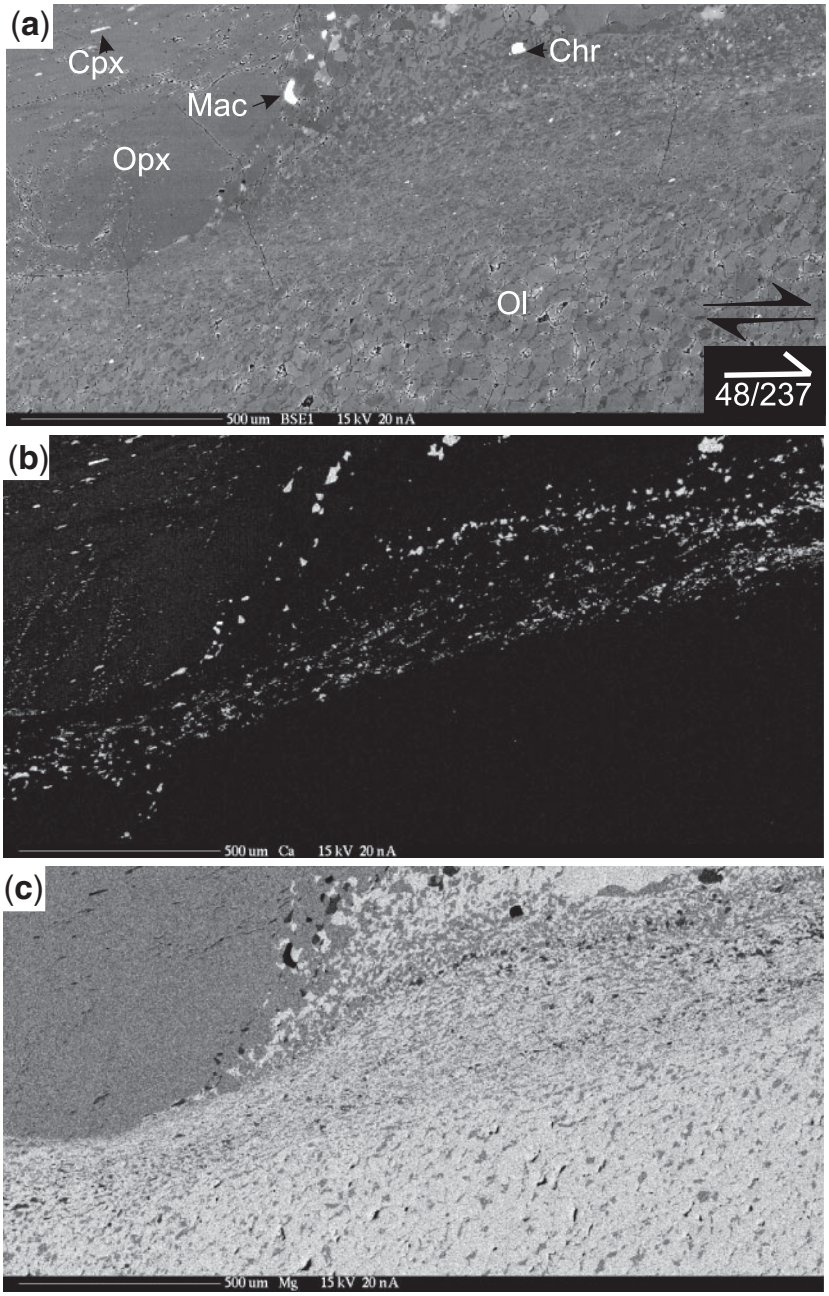

Fig. 7. Microstructural and phase relationships adjacent to orthopyroxene porphyroclast in NC07-16f. (a) Backscatter image. (b) Ca-element map. (c) Mg-element map. It should be noted that abundant fine orthopyroxene is intermingled with olivine adjacent to the porphyroclast, without other phases present. Amphibole is present in increasing abundance in the very fine-grained part of the shear zone (particularly visible in (b)). The presence of minor amounts of the sulfide macktinawite (Mac) attests to incipient serpentinization. Clinopyroxene (Cpx) is present only as exsolution lamellae in the porphyroclast. Ol, olivine; Opx, orthopyroxene; Chr, chrome spinel.

thin sections were subjected to further chemical–mechanical polishing for ~20 min with colloidal silica and very thinly carbon-coated to prevent specimen charging. EBSD data were collected using HKL CHANNEL5 software with both a Hitachi S3400N SEM at the University of Wisconsin–Madison, and with a FEI Quanta 600 FE-SEM at Texas A&M University. A general description of this method has been provided by Prior *et al.* (1999).

Crystallographic orientation data were collected using a variety of step sizes, depending on the grain size of the material of interest. Patterns were collected relatively slowly, to maximize quality, and indexed on the basis of

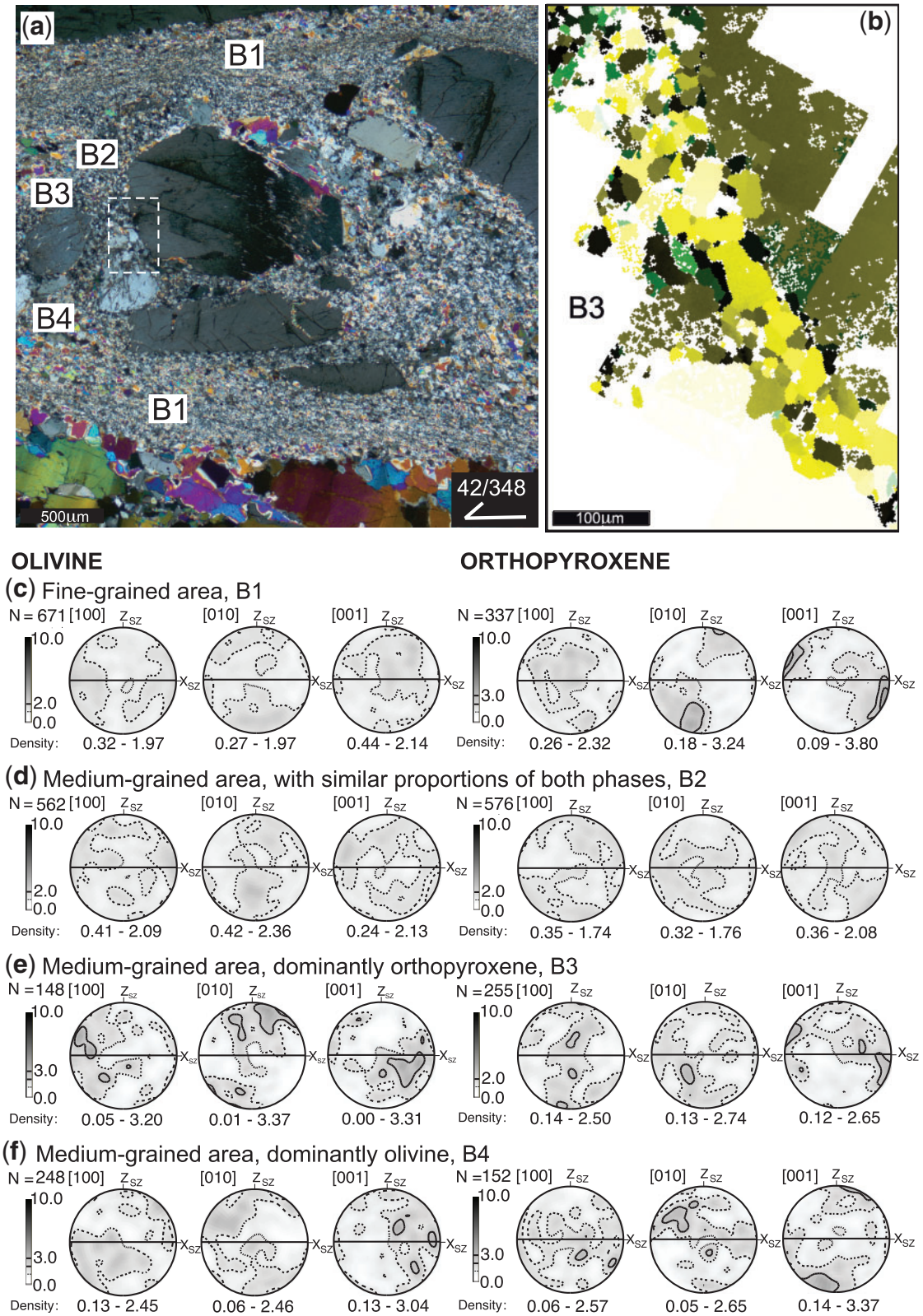

Fig. 8. (a) Photomicrograph illustrating a section of the shear zone in sample NC07-l6c2 in which the finest-grained regions bifurcate around orthopyroxene porphyroclasts. Section is cut approximately perpendicular to the shear zone boundary and to the lineation (Y–Z section). (b) EBSD map of area between orthopyroxene porphyroclasts. Location indicated by dashed rectangle in (a). Grains are coloured according to phase (green indicates olivine; yellow indicates orthopyroxene). Within these colour ranges, grains are shaded according to Schmid factor calculated for loading at 45° to the shear plane (horizontal in this image) on (010)[100] for olivine and (010)[001] for pyroxene. Darker shades represent lower Schmid factors. The fine-grained, high Schmid factor, small orthopyroxene grains between the porphyroclasts should be noted. (c–f) Pole figures illustrating LPO of olivine and orthopyroxene, derived from one point per grain of map data over the area illustrated in (a). The plots represent different domains, separated according to grain size and proportion of olivine:orthopyroxene. Plots are equal area, lower hemisphere. Z_{SZ} is the pole to the shear zone boundary; the slip vector is parallel to X_{SZ}. Contouring is multiples of uniform density.

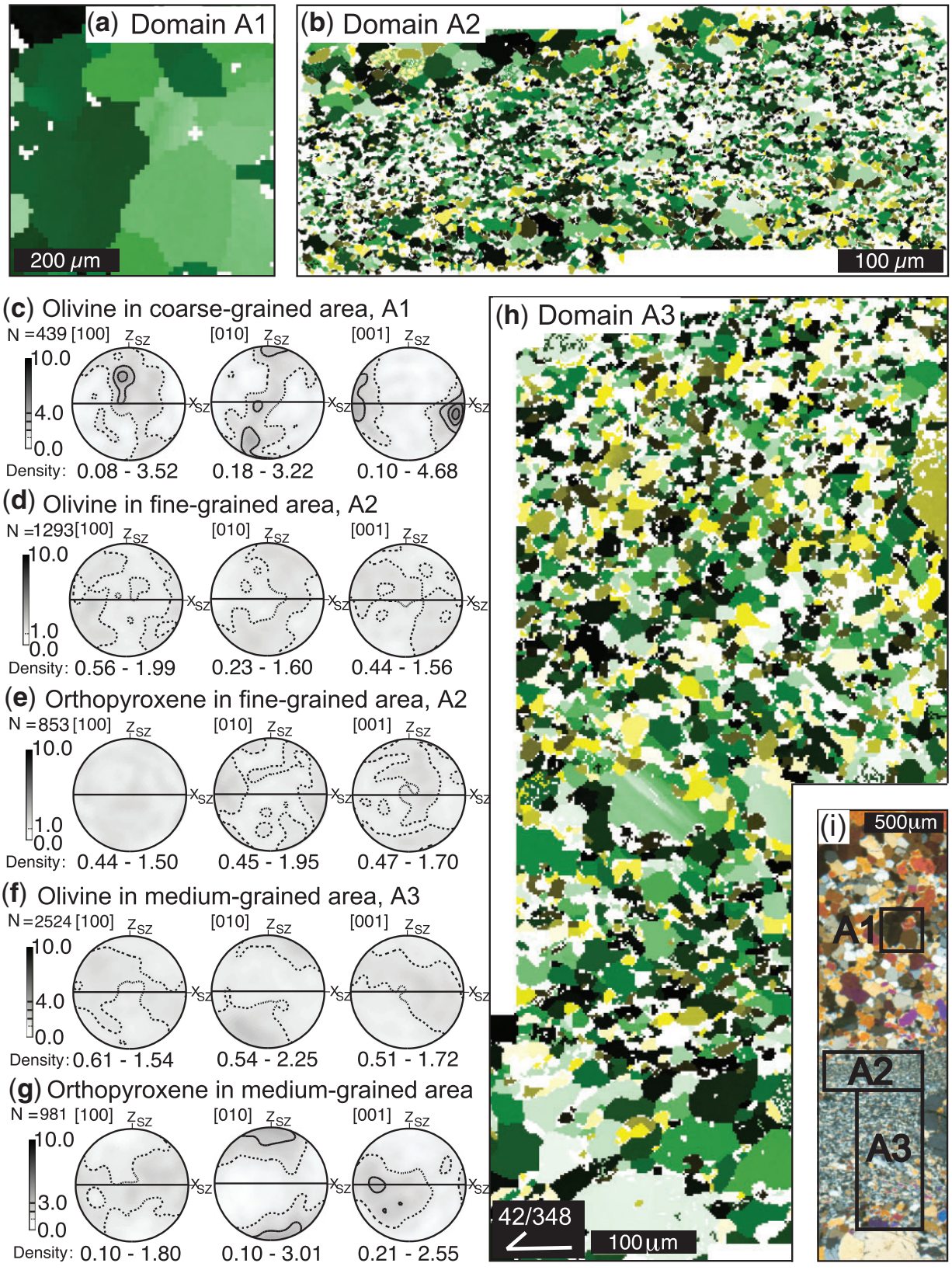

Fig. 9. (a, b, h) EBSD maps of different grain size domains from sample NC07-16c1. The scale change from (a) to (b) and (h) should be noted. Grains are coloured according to phase (green indicates olivine; yellow indicates orthopyroxene). Within these colour ranges, grains are shaded according to Schmid factor calculated for loading at 45° to the shear plane (horizontal in this image) on (010)[100] for olivine and (010)[001] for pyroxene. Darker shades represent lower Schmid factors. (a) is only part of the mapped area of this grain size domain. (c–g) Pole figures illustrating LPO of olivine and orthopyroxene, derived from one point per grain of the map data in (a), (b) and (h). Plots are equal area, lower hemisphere. Z_{SZ} is the pole to the shear zone boundary; the slip vector is parallel to X_{SZ}. Contouring is multiples of uniform density. (i) Photomicrograph, taken under crossed polarizers, illustrating the relative locations of the EBSD maps in (a), (b) and (h).

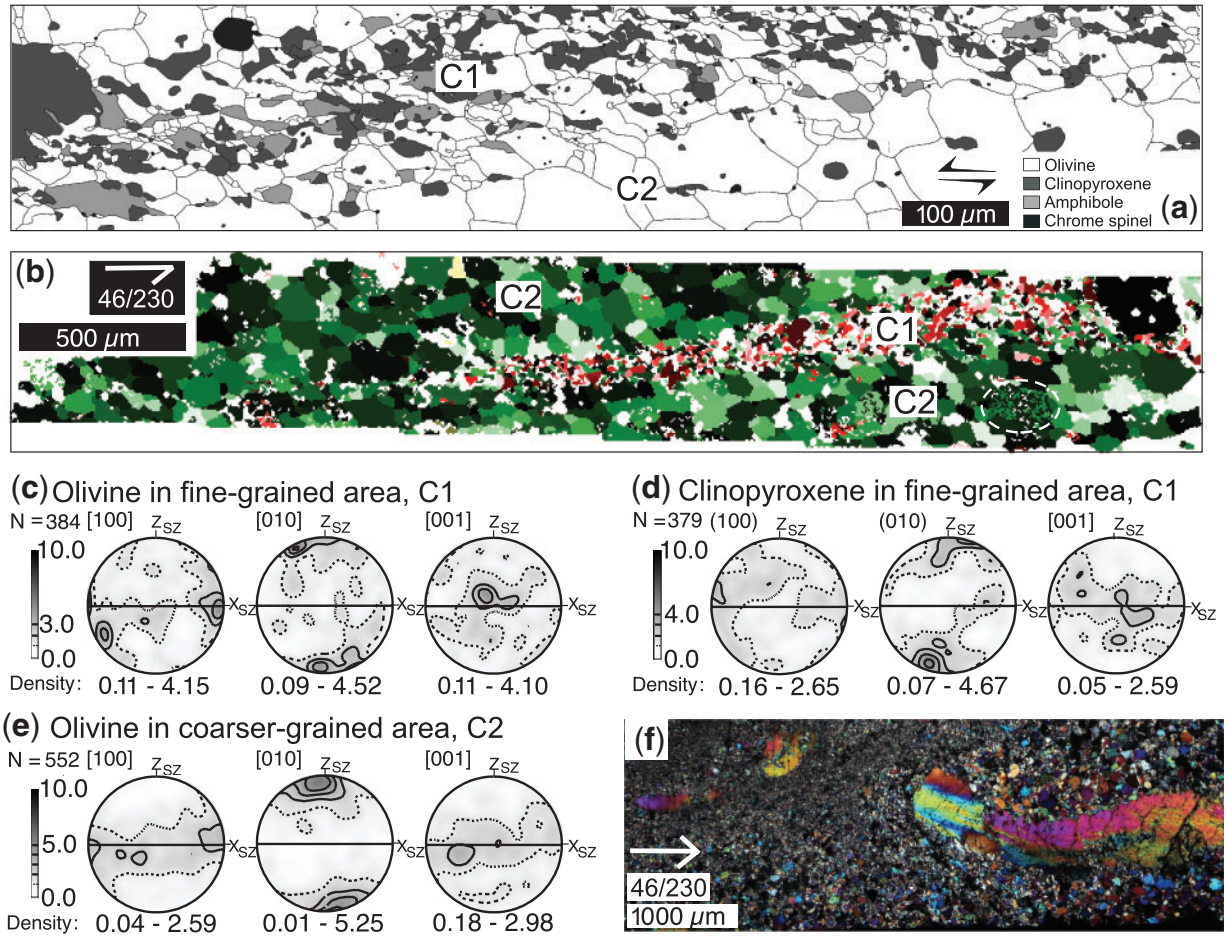

Fig. 10. Sample NC07-16a. (a) False-coloured microstructural map constructed from traced backscatter images of decorated samples of a fine-grained mixture of olivine, clinopyroxene, amphibole and chrome spinel in the tail of a porphyroclast. (b) EBSD map in which grains are coloured according to phase (green indicates olivine; red, clinopyroxene; yellow, orthopyroxene). Within these colour ranges, grains are shaded according to Schmid factor calculated for loading at 45° to the shear plane (horizontal in this image) on (010)[100] for olivine and (010)[001] for pyroxenes. Darker shades represent lower Schmid factors. Grains containing multiple indexed solutions (e.g. grain within dashed white ellipse) were excluded from LPO plots. (c–e) Pole figures illustrating LPO of olivine and clinopyroxene, derived from one point per grain of the map data in (b), and, for (c) and (d), from a higher-resolution map of the fine-grained material (not shown here). Plots are equal area, lower hemisphere. Z_{SZ} is the pole to the shear zone boundary; the slip vector is parallel to X_{SZ}. Contouring is multiples of uniform density. (f) Photomicrograph of a foliation-parallel (X–Y) section of this sample, illustrating elongate pyroxene porphyroclasts in a fine-grained matrix. Crossed polarizers.

≥5 Kikuchi bands so that only a limited (≪1%) amount of mis-indexing of crystal orientation could have occurred. Resultant data collection rates were one point every 0·4–0·9s. Data were processed (see Bestmann & Prior, 2003) to produce microstructural maps and orientation datasets based on one point per grain, where grains are separated by boundaries with misorientations ≥10°. Grains containing at least three analysis points (ie. ≥2·5 times the step size in diameter) were selected for plotting on pole figures. This sampling scheme produces data directly comparable with those collected by universal stage techniques (e.g. Webber *et al.*, 2008).

LPOs of olivine and pyroxenes in the host-rock and shear zone are illustrated in Figs 4, 8, 9 and 10. All LPO fabric plots were generated using the program *PFCh5.app* courtesy of D. Mainprice, and are presented on lower hemisphere equal area stereographic projections in the $X_{H/SZ}$–$Y_{H/SZ}$–$Z_{H/SZ}$ reference frame defined previously. The pole figures are oriented so that the view is down, into the shear zone, towards the NW. Fabric strengths are indicated by the density range indicated beneath each of the contour plots. All map data are coloured to represent phase and shaded to represent the Schmid factor (maximum normalized resolved shear stresses) on typical slip systems in that mineral (as indicated in the figure captions), for loading at 45° to the shear zone boundary. These Schmid factors were calculated by the HKL CHANNEL5 software.

Lattice preferred orientations

Host-rock

The host-rock olivine has a stronger LPO than any of the shear zone materials. The LPO (Fig. 4b) has a [100]-maximum subparallel to X_H and a [010]-maximum subparallel to Z_H; [001] are distributed in a very diffuse girdle perpendicular to X_H.

Monophase domain

LPO strengths in intermediate-grained monophase olivine on the margins of the shear zone (Domains A1 and C2) are intermediate between those of the host and the fine-grained polyphase regions (such as Fig. 9b).

The olivine grains in the monophase domains adjacent to the orthopyroxenite dike and the clinopyroxenite dike yield different LPOs. Near the orthopyroxenite dike (NC07-16c1), there is a strong axial concentration of [001] parallel to X_{SZ}, a weak girdle of [100] along the Y_{SZ}–Z_{SZ} plane with a concentration midway between Z_{SZ} and Y_{SZ}, and a weak girdle of [010] along the Y_{SZ}–Z_{SZ} plane with a concentration parallel to Z_{SZ} (Fig. 9c).

In NC07-16a (near the clinopyroxenite dike), the monophase olivine has an LPO (Fig. 10e) similar to that observed in the host. In particular, there is a strong axial concentration of [010] parallel to Z_{SZ}. However, unlike the host, [100] and [001] spread in a girdle along the X_{SZ}–Y_{SZ} plane, with only weak concentrations of [100] parallel to X_{SZ} and [001] midway between X_{SZ} and Y_{SZ}.

Polyphase domain, near and between offset orthopyroxenite dike

In the polyphase domain between the offset orthopyroxenite dike, where varying proportions of orthopyroxene are mixed into the shear zone, there are a variety of different olivine and orthopyroxene LPOs. In NC07-16c1 (Fig. 9d–f), both olivine and orthopyroxene LPOs are essentially random. However, where moderately fine-grained olivine and orthopyroxene are mixed in near equal proportions (Fig. 9, Domain A3), orthopyroxene has one of the strongest LPOs of the shear zone materials. This LPO (Fig. 9g) has an axial concentration of [010] parallel to Z_{SZ}.

In NC07-16c2 (Fig. 8c–f), the olivine LPOs are also essentially random. The weakest LPO within the analysed samples is derived from Domain B3, where olivine is modally least abundant (Fig. 8e). Orthopyroxenes in this sample also generally have very weak crystallographic fabrics. However, the orthopyroxene LPOs are stronger than in intermixed olivine, and approach those observed in intermediate-grained olivine in the monophase domain. The strongest orthopyroxene LPO is derived from Domain B1 (Fig. 8c), which is the finest-grained part of the shear zone in this section. The orthopyroxenes display two different, resolvable LPOs. In the finest-grained part of the shear zone (Domain B1; Fig. 8c) there is an [010] axial concentration near Z_{SZ}, and an [001] concentration near X_{SZ}. Conversely, in the olivine-dominated region (Domain B4; Fig. 8f), there is an [001] axial concentration near Z_{SZ}.

Polyphase domain, near clinopyroxenite dike

In the shear zone adjacent to the clinopyroxenite dike (NC07-16a), the olivine LPO in the fine-grained mixture of olivine, clinopyroxene and amphibole in the tail of clinopyroxene porphyroclasts has an axial concentration of [010] at Z_{SZ}, and weaker axial concentrations of [100] at X_{SZ} and [001] at Y_{SZ} (Fig. 10c). Clinopyroxenes in this sample have poles to (010) strongly clustered around Z_{SZ}. [100] are slightly concentrated near X_{SZ}, and poles to (001) near Y_{SZ}, but both also form partial girdles in the X_{SZ}–Y_{SZ} plane.

KINEMATICS AND DEFORMATION MECHANISMS

Calculation of slip vector

A unique slip vector cannot be found from field relationships of the offset dikes, as they do not converge to define a single piercing point. A weak elongation of pyroxene porphyroclasts visible in foliation-parallel sections, trending towards 230°, and pitching 54° ± 10°SE in the shear zone (Fig. 10f), is interpreted as the orientation of the slip vector, X_{SZ}. This slip vector orientation is also consistent with the LPO data. The strongest LPOs in the polyphase domain of the shear zone are found in orthopyroxene neoblasts (Fig. 8c and e). Orthopyroxene LPOs observed in experimental data and other natural shear zones indicate that slip occurs parallel to [001] in this mineral (Christensen & Lundquist, 1982; Skemer *et al.*, 2006). We obtain a point maximum of [001] parallel to the direction of elongation of the porphyroclasts, which would indicate slip parallel to this crystallographic direction. Consistent LPOs are also observed in olivine in the monophase domain for this reference frame (Figs 9c and 10e; described in the preceding section).

The orthopyroxenite dike orientation varies from footwall to hanging wall because it is folded. Combined with the possible error in the slip vector from the LPO data, this makes interpretation of the true shear sense and slip vector difficult solely from geometric relationships observed in outcrop. However, oblique grain shape fabrics and sigmoidal shear sense indicators in X_{SZ}–Z_{SZ} sections (Figs 3, 5 and 10), coupled with asymmetry of olivine and pyroxene LPOs, indicate a sinistral normal sense of displacement across the zone. It should be noted that pyroxene has [010] and [100] maxima back-rotated with respect to the sense of shear as predicted by Bascou *et al.* (2002). The true shear sense is opposite to the sense of offset of the orthopyroxenite dike observed in outcrop (Fig. 2), hence

this offset must be apparent and result from juxtaposition of segments of the folded orthopyroxenite dike with different orientations in the footwall and hanging wall at the outcrop face. Slip is subparallel to the intersection of the orthopyroxenite dike with the shear plane, so the true slip is greater than 21 cm (Fig. 2f). Because the shear zone is <5 mm thick, assuming simple shear, γ (simple shear strain) postdating formation of the orthopyroxenite dike exceeds 42.

Deformation mechanisms

Host-rock

The host-rock microstructures indicate dislocation creep of olivine aggregates. Undulose extinction is formed by a combination of glide and limited recovery by dislocation climb (Poirier & Guillopé, 1979). These processes accommodated the intracrystalline strain that resulted in formation of a grain shape-preferred orientation. The interlobate grain boundaries also indicate that strain-induced grain boundary migration operated. The smaller grains that sometimes decorate the boundaries between the larger grains represent neoblasts formed during dislocation creep. The relatively strong LPO implies that glide occurred on (010)[100], which also suggests that dislocation creep was the dominant deformation mechanism. The (010)[100] system is that most commonly reported to be activated under conditions that would realistically be realized in the Earth's upper mantle in both experimental (e.g. Kohlstedt & Goetze, 1974; Nicolas & Poirier, 1976; Mercier, 1985; Bai *et al.*, 1991; Bai & Kohlstedt, 1992) and natural examples (e.g. Boudier & Coleman, 1981; Strotzki *et al.*, 1990; Vissers *et al.*, 1995; Ben Ismaïl & Mainprice, 1998). Hence, we infer the host-rock tectonite fabric was imposed during plastic flow in the upper mantle, before emplacement of the Twin Sisters massif at the surface.

The orthopyroxene microstructures within the dike indicate that deformation of this mineral aggregate was accommodated by kinking and bending on twin planes, along with recrystallization to small, new grains along these high-strain sites. Etheridge (1975) described similar microstructures from the Giles Complex, central Australia, and interpreted the kinking to result from glide on (001), indicating that the predominant deformation mechanism was crystal plasticity. On the other hand, these microstructures are also similar to those observed in other minerals at the transition from semi-brittle processes to dislocation creep (e.g. in feldspar; Tullis & Yund, 1987; or biotite; Etheridge & Hobbs, 1974), so we cannot discount the possibility that similar semi-brittle processes may have operated during shear zone initiation in our case.

Monophase domain

The coarser olivine grains in the monophase domain have a grain shape fabric (Fig. 3a) suggesting that they experienced deformation by dislocation creep.

The LPO observed in this domain in NC07-16a (near the clinopyroxenite dike; Fig. 10e) is consistent with glide on (010)[100], similar to the slip system suggested by the host-rock LPO (Fig. 10e). Because the fabric is resolved in a different reference frame from that in the host-rock, it is unlikely that the fabric is inherited. This deformation probably occurred at similar conditions to those under which the host-rock fabric was developed, consistent with nucleation of the shear zone as a result of a stress heterogeneity during bulk deformation of the massif. However, the fact that most of these grains have very little undulose extinction and relatively straight grain boundaries indicates that they experienced some recovery, resulting in organization of intracrystalline dislocations into low-energy configurations.

The LPO observed in this domain in NC07-16c1 (near the orthopyroxenite dike; Fig. 9c) indicates that glide occurred on (010)[001]. One possible interpretation for this slip system is that deformation in this domain, near the orthopyroxenite dike, occurred in the presence of water ['Type B' LPO; Jung & Karato (2001)]. However, as this LPO is not observed in other monophase domain olivine aggregates, this interpretation would imply variations in water fugacities over small distances, which is difficult to explain. Similar LPOs have also been observed in deformed aggregates of olivine + orthopyroxene (Sundberg & Cooper, 2008) or of olivine + melt (Holtzman *et al.* 2003), but neither of these situations is likely to have been realized during deformation in this monophase olivine domain.

Polyphase domain

Within the fine-grained, mixed phase material in the centre of the shear zone, alignment of grain and phase boundaries between multiple grains, parallel to the shear plane, indicates that some deformation was accommodated by co-operative grain boundary sliding (Raj & Ashby, 1971). Similar microstructures were described by Newman *et al.* (1999) from natural peridotites that they inferred had deformed by grain-size-sensitive creep, and by Sundberg & Cooper (2008) in experimentally deformed olivine–orthopyroxene aggregates. The latter, experimental samples, exhibited rheological behaviour characterized by a stress exponent approaching unity, suggesting that grain-size-sensitive (linear viscous) creep was also the dominant deformation mechanism in these polyphase aggregates.

Weakening of an LPO, as is observed in olivine in these fine-grained polyphase aggregates, is also commonly associated with operation of grain-size-sensitive deformation mechanisms (e.g. Fliervoet *et al.*, 1999; Warren & Hirth, 2006; Skemer & Karato, 2008). Furthermore, the finest recrystallized grain sizes we measured (olivine $\bar{D} = 4{\cdot}6$ μm; orthopyroxene $\bar{D} = 4{\cdot}8$ μm) are similar to the grain size developed in the experimentally deformed samples described by Sundberg & Cooper (2008), which

experienced grain-size-sensitive creep, and the minimum grain sizes are also similar to those reported by Newman *et al.* (1999) in natural aggregates that they argued were deformed by grain-size-sensitive creep. Thus, we conclude that grain-size reduction during deformation in our samples resulted in a transition to grain-size-sensitive creep, leading to strain-softening and promoting further localization of deformation (Twiss, 1976; Rutter & Brodie, 1988; de Bresser *et al.*, 1998, 2001).

Grain and phase boundaries in our samples become less well-aligned with increasing grain size, suggesting that another mechanism apart from grain-size-sensitive creep, such as intracrystalline plasticity, accommodated some of the strain in the coarser polyphase aggregates. However, the only olivine that contains an LPO that may have formed by these processes is in the fine-grained mixture of olivine, clinopyroxene and amphibole in the tail of clinopyroxene porphyroclasts, adjacent to the clinopyroxenite dike (NC07-16a). This LPO is characteristic of glide on (010)[100].

On the other hand, all pyroxenes within this domain have LPOs. Although LPO development has been observed during diffusion creep (Sundberg & Cooper, 2008), the resulting LPOs are dissimilar to those observed in our samples. Instead, the presence of LPOs in our samples suggests that some deformation of orthopyroxene was accommodated by intracrystalline plasticity. Near the orthopyroxenite dike, the orthopyroxene LPO in NC07-16c1 (Fig. 9g) indicates that (010) is a preferred glide plane during dislocation creep of this mineral but it is less clear what glide direction was operative. In the finest-grained part of the shear zone (NC07-16c2; Domain B1; Fig. 8c) and where orthopyroxene is modally dominant (NC07-16c2; Domain B3; Fig. 8e), the orthopyroxene LPOs indicate that glide occurred on (010)[001]. There are only a few other reports of glide on (010) in naturally deformed orthopyroxene (Jackson, 1961; Ave'Lallemant, 1967; Carter *et al.*, 1972; Naze *et al.*, 1987). However, we note that glide also occurred on (010) in clinopyroxene in other parts of the polyphase domain of the shear zone. In the olivine-dominated region (NC07-16c2; Domain B4; Fig. 8f) the orthopyroxene LPO suggests that (001) was the dominant glide plane. This pole figure, however, is derived from a small number of grains ($N = 152$) and we do not attach a high level of confidence to this latter interpretation.

Adjacent to the clinopyroxenite dike (NC07-16a), clinopyroxene LPOs in the polyphase domain indicate that glide occurred on (010) (Fig. 10d), but a single dominant slip direction is not clear from the data. Partial girdles in the X_{SZ}–Y_{SZ} plane in these samples are similar to S-type fabrics reported for natural eclogites (Helmstaedt *et al.*, 1972), which have been suggested to result from activity of slip on {110} and {1–10} (Ulrich & Mainprice, 2005, and references therein). However, Ulrich & Mainprice (2005) showed that the dominant control on formation of these 'S-type' rather than 'L-type' fabrics is an increase in the ratio of pure:simple shear, not variation in activity of these subsidiary slip systems.

GEOTHERMOMETRY AND MINERAL CHEMISTRY

Microprobe analytical techniques

Mineral compositional data were obtained using quantitative wavelength-dispersive spectrometry (WDS) methods on a four-spectrometer CAMECA SX50 electron microprobe at Texas A&M University. Samples were prepared as oriented thin sections, polished, and coated with ~15 nm of carbon. The microprobe was operated using a beam current of 10 nA, an accelerating voltage of 15 kV, and a beam diameter of 1 μm (olivine, pyroxene, spinel) or 5 μm (amphibole). Counting times ranged from 20 to 120 s, but were mostly 30–60 s, with longer times for minor elements to improve counting statistics. These chemical data are presented in Supplementary Data Table S1 (available for downloading at http://www.petrology.oxfordjournals.org/). For grains smaller than 100 μm, we report the average of 1–3 analyses. For larger grains of pyroxene, spinel and amphibole, where composition commonly varies across grains as a result of zoning, we report single analyses. No significant variation in composition was observed within olivine grains, so up to 10 analyses were averaged from each grain of this mineral.

Normalized mineral formulae for olivine, spinel and pyroxenes were calculated on the basis of a fixed number of cations (three for olivine and spinel; four for pyroxenes). Amphibole formulae were determined using the iterative procedure described by Lamb & Popp (2009). This procedure requires a value of Fe^{3+}/Fe_{total} ($Fe_{total} = Fe^{3+} + Fe^{2+}$) but, because we lack this information, we have assumed an end-member case, where $Fe^{3+}/Fe_{total} = 0$. An empirical relation to cation content, described by Popp *et al.* (1995), was used to calculate the oxy-content of the amphiboles. Given these constraints, and by requiring charge balance, the Lamb & Popp (2009) procedure can be used to determine the amount of vacancy in the A crystallographic site and, therefore, a unique amphibole formula can be determined.

Mineral chemistry

The chemical compositions of amphibole, spinel, orthopyroxene, and clinopyroxene are relatively variable, and this variation is, to some extent, correlated with various microstructural domains (Fig. 11). However, some of this compositional variation may relate to sample location, as NC07-16f, from adjacent to the orthopyroxenite dike, has primarily orthopyroxene porphyroclasts in the shear zone, whereas NC07-16a, from adjacent to the

clinopyroxenite dike, has primarily clinopyroxene porphyroclasts. This difference may impart a chemical variation between the two samples that may otherwise mask compositional trends between the microstructural settings. Here we focus on the compositions of grains in the host-rock (including the cores of porphyroclasts within the shear zone) versus the finer grains in the shear zone to illustrate the relation between mineral composition and microstructural setting.

Pyroxenes

These minerals exhibit distinct compositional differences between the host-rock and shear zone. Figure 11a and b shows plots of Mg/(Mg + Fe) vs Ca content of the pyroxenes (the Ca content is given as atoms per formula unit; a.p.f.u.). The clinopyroxene within the finer-grained polyphase domain is progressively enriched in both Ca and Mg/(Mg + Fe) with respect to the host compositions. Conversely, orthopyroxene from the finer-grained shear zone has smaller amounts of Ca and Mg/(Mg + Fe) as compared with that in the host-rock.

Chrome spinel

All the analysed spinels are Cr-rich with $70 < X_{Cr} < 80$ and $30 < X_{Mg} < 50$. Intermediate and fine-grained spinels in the shear zone have higher Al/(Al + Cr) and lower Mg/(Mg + Fe) as compared with both spinel porphyroclasts and host-rock spinel grains (Fig. 11c). The decrease in Cr:Al within the finer grains indicates evolution from a chrome spinel towards a more aluminium- and iron-rich spinel. We were unable to obtain many analyses from very fine spinels within the shear zone, as they are generally only 1–2 μm in diameter (see Table 1), similar to the microprobe beam diameter. However, optically these grains are less opaque than both spinel porphyroclasts and host grains, and this change in optical properties is consistent with decreasing Cr contents.

Amphibole

The chemical trends are less clear in amphiboles. Both host-rock and shear zone contain amphiboles with a tremolitic composition, with ~3 wt % Al_2O_3 and <1 wt % Na_2O. However, many host-rock amphiboles have higher Al contents than shear zone amphiboles, and grains intermixed with clinopyroxene in clinopyroxene porphyroclast tails in NC07-16a are pargasitic with 10–13 wt % Al_2O_3 and ~2·9 wt % Na_2O (Fig. 11d).

Geothermometry

Temperatures were estimated from the chemistries of minerals in textural equilibrium in the various microstructural domains of the samples using the olivine–spinel thermometer of Ballhaus *et al.* (1991) and the two-pyroxene thermometer of Taylor (1998) (Table 2). The samples do not contain suitable assemblages for geobarometry, so we cannot constrain pressure. However, spinel lherzolites such as we observe are stable in the pressure range ~0·6–1·4 GPa below 1000°C (Gasparik, 1987), so we have assumed an average pressure of 1 GPa. If the rocks equilibrated at lower pressures, our calculated temperatures are marginally too high. For example, at 0·5 GPa, temperatures estimated using the Ballhaus *et al.* (1991) thermometer are 5–6°C lower than those we report in Table 2, whereas those from the Taylor (1998) thermometer are 12–14°C lower.

Comparison between the temperature inferred from the two-pyroxene geothermometer of Taylor (1998) and the temperature of experimentally equilibrated natural peridotite samples indicates that this two-pyroxene geothermometer is subject to an uncertainty of ±31°C at the 1σ level (Taylor, 1998). This estimate, combined with the uncertainty in the value of *P*, yields an estimated uncertainty for the two-pyroxene geothermometer of ±50°C. However, some portion of this uncertainty must arise from systematic errors, and thus the relative temperature differences are more accurate than these absolute values. Balhaus *et al.* (1991) did not attempt to estimate uncertainties for the olivine–spinel thermometer, and this geothermometer has not been subjected to the same experimental verification that has been applied to the two-pyroxene and other geothermometers. In cases in which both two-pyroxene and olivine–spinel temperature estimates are available in the same sample, both geothermometers yield similar relative differences. Therefore, we have included estimated temperatures based on olivine–spinel as a guide to the temperature of mineral equilibration in those samples where temperatures based on two-pyroxene geothermometry are unavailable.

Host-rock

In NC07-16a (near the clinopyroxenite dike), the two thermometers (two-pyroxene and olivine + spinel) yield consistent temperature estimates of ~760–780°C. This agreement between different thermometers that are based on different mineral pairs is evidence that minerals in the host-rock equilibrated at temperatures approaching ~800°C. In the host-rock near the orthopyroxenite dike (NC07-16f), the two thermometers provide estimates of equilibration temperature in the host-rock that differ by ~90°C. The temperature estimated using the two-pyroxene thermometer (720°C) is similar to that estimated from the compositions of porphyroclasts and exsolution lamellae within them. Furthermore, the clinopyroxene grain from which this temperature estimate was made contains amphibole inclusions, which may have originated as exsolution lamallae. It is possible that the average clinopyroxene composition in this case has been modified, possibly during early deformation, so that the estimated temperature is lower than that estimated from the host-rock of sample NC07-16a. Furthermore, three

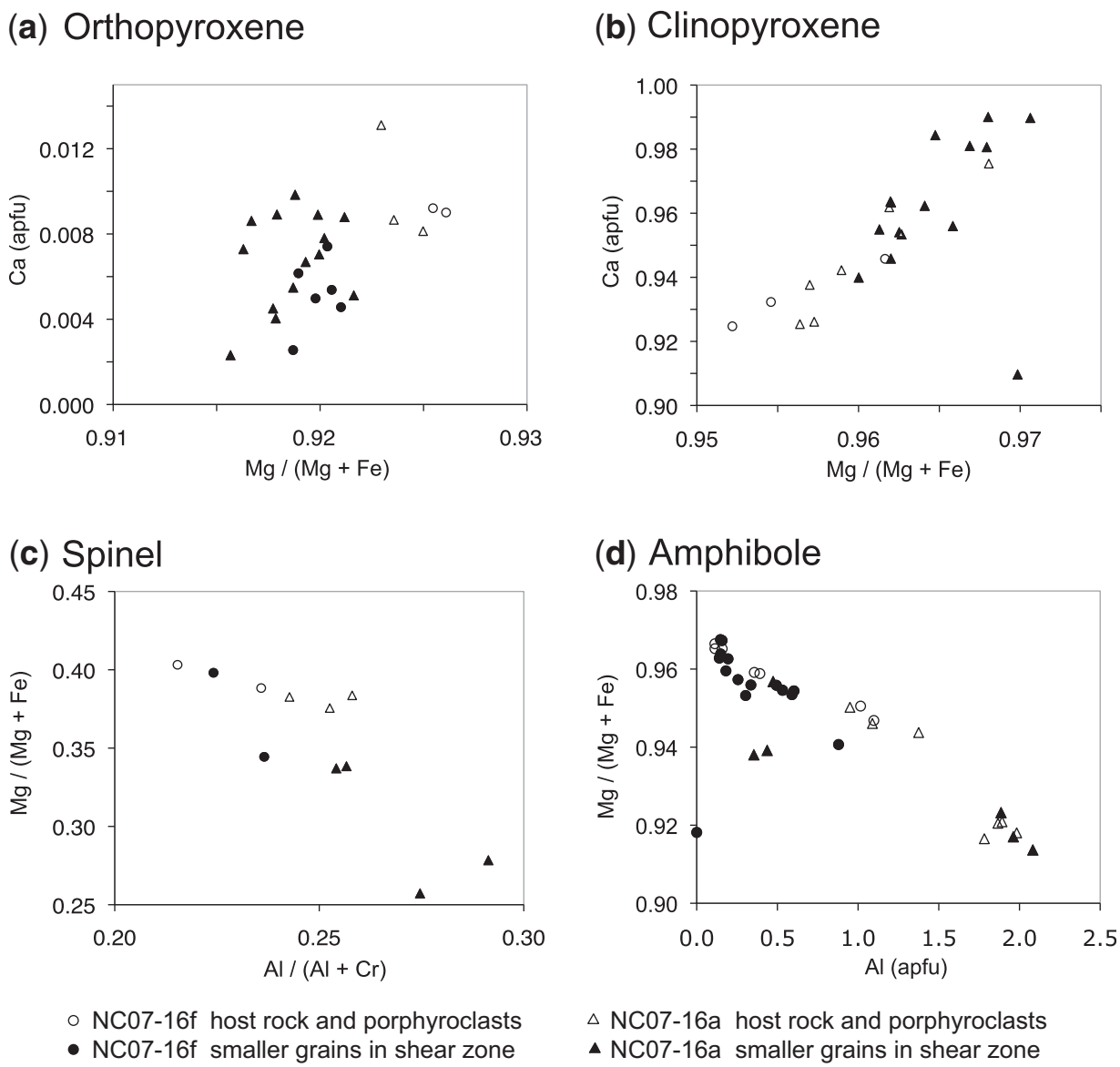

Fig. 11. Plots illustrating evolution of element ratios during production of fine-grained material in the shear zone from coarse porphyroclasts and host-rock. Sample NC07-16f has primarily orthopyroxene in the shear zone. Sample NC07-16a has primarily clinopyroxene. The amphibole compositions plotted in (d) are based on mineral formulae calculated for $Fe^{2+} = Fe^{T}$.

olivine–spinel pairs from the host-rock near the orthopyroxene dike (NC07-16f) all yield a temperature of 810°C. We infer that a temperature of ~800°C is the best estimate of the temperature at which the host-rock experienced pervasive metamorphic equilibration.

Monophase domain

In NC07-16f (near the orthopyroxenite dike) temperatures were estimated from intermediate-grained shear zone spinel and olivine (~660°C). Spinels with this grain size are found only within the shear zone, so this temperature estimate is likely to be representative of shear zone deformation temperatures. In NC07-16a (near the clinopyroxenite dike), intermediate-grained olivine equilibrated with spinel at ~750°C. Pyroxenes on the boundary of this domain with the host-rock yield temperatures of ~690°C.

Polyphase domain

In NC07-16f (near the orthopyroxenite dike), a spinel porphyroclast and adjacent fine-grained olivine gave a temperature of ~730°C. Unfortunately, fine-grained spinels in the shear zone are too small (<2 μm diameter; Table 1) to obtain reasonable analyses. Points analysed in a transect

Table 2: Geothermometric estimates (values in °C) from host-rock and shear zone materials

Sample number	Host-rock		Shear zone			
	Olivine–spinel*	2-pyx†	Intermediate-grained; margin of zone		Fine-grained	
			Olivine–spinel	2-pyx	Olivine–spinel	2-pyx
NC07-16a	780	760	750	690	640	670
	780	780			660	
		760				
NC07-16f	810	720	660		730	
	810					
	810					

*Ballhaus *et al.* (1991).
†Taylor (1998).
Subsequent rows under the same heading indicate estimates from different mineral pairs in the same sample and microstructural setting.

across the spinel porphyroclast did not yield a pattern of core–rim zoning. The geothermometric estimate was made from analyses from within 100 μm of the porphyroclast rim, and surrounding fine-grained olivine.

In NC07-16a (near the clinopyroxenite dike) the fine-grained material within the shear zone yields temperatures of 640°C using the olivine–spinel thermometer and 670°C using the two-pyroxene thermometer.

DISCUSSION

Conditions of deformation

The evidence outlined above allows us to constrain the conditions of deformation of the ultramafic ultramylonite, as summarized below.

Kinematics and timing

In the outcrop face illustrated in Fig. 2a, there appears to be marked change in the amount of offset of the orthopyroxenite and clinopyroxenite dikes along the shear zone. This observation is surprising because the orientations of the two dikes are very similar. Furthermore, the shear zone terminates very rapidly laterally and appears to have a displacement:length ratio of the order of 0·4. Microstructural observations indicate that both the pyroxenite dikes were deformed by solid-state mechanisms, so most displacement on the shear zone probably occurred after intrusion of the clinopyroxenite dike. There are two remaining options to explain the observations: either (1) the smaller offset of the clinopyroxenite represents decreased slip near the edge of the shear zone or (2) both dikes are offset a similar amount, but the orthopyroxenite appears to have greater offset as it is non-planar. We cannot evaluate between these options.

The total slip exceeds 21 cm, as noted above, giving $\gamma > 42$ for the <5 mm wide zone. Hence, this shear zone accommodated a very high strain, comparable with the highest published shear strain estimates in crustal rocks (e.g. Boullier, 1986; Gilotti & Hull, 1990; Lacassin *et al.*, 1993; Norris & Cooper, 2003). Similar high strains have also recently been measured along narrow zones in ultramafic rocks in the Red Hills massif (Webber *et al.*, in preparation). The shear zone therefore provides another valuable natural example of how microstructures and LPO evolve during very-high strain deformation (see Toy *et al.*, 2008).

Deformation mechanisms

A major finding is that the deformation mechanism varies in the shear zone. The monophase domain olivines have a grain shape fabric and LPOs indicating that they experienced deformation by dislocation creep. In contrast, polyphase domain minerals, which display nearly random LPOs and smaller grain sizes, are interpreted to have deformed by grain-size-sensitive creep. These fabrics may have formed concurrently, but differ because of the mixed phases in the polyphase domain. It is likely that a fine grain size within the polyphase domain, suitable for activation of grain-size-sensitive creep mechanisms, was stabilized by pinning of grain boundaries (e.g. Herwegh & Kunze, 2002).

Temperature and pressure estimates

The temperature estimates reported in Table 2 indicate that the host-rock equilibrated at temperatures in the approximate range 760–810°C. Experimental data (Ave'Lallemant & Carter, 1970) indicate that olivine

should experience a transition from (010)[100]-glide (as observed in the host-rock) to {0kl}[100] and then {110}[001]-glide at lower deformation temperatures. The LPO characteristic of glide on (010)[100] has been reported most commonly from natural peridotites deformed at upper mantle conditions, in the temperature range 900–1200°C (e.g. van der Wal & Vissers, 1993; Dijkstra *et al.*, 2001, 2002), whereas glide parallel to [001] has been reported from natural samples deformed in the temperature range 700–900°C (e.g. Gueguen & Nicolas, 1980; Vissers *et al.*, 1995). Thus, the temperatures estimated from geothermometry seem lower than those at which we would expect the LPO in these materials to have developed, by comparison with other natural examples. Alternatively, if we extrapolate the experimental results of Carter & Ave'Lallemant (1970) to realistic natural strain rates of 10^{-11} to 10^{-13} s^{-1}, (010)[100]-glide should be observed down to temperatures of 700–800°C. This interpretation is consistent with our results. Therefore, we infer that the olivine LPO in the host-rock formed at temperatures of around 800°C or greater.

Because metamorphic equilibration proceeds most rapidly in deforming materials, we expect the geothermometric estimates from minerals that underwent syn-deformational reaction to reflect deformation temperatures. The temperature estimates reported in Table 2 indicate that the shear zone was active between ~650 and 750°C. There is no consistent variation between temperatures estimated in the marginal and central domains of the shear zone.

The observed orthopyroxene LPOs indicate that glide occurred on the (010) plane. Jackson (1961), Ave'Lallemant (1967), Carter *et al.* (1972) and Naze *et al.* (1987) have reported orthopyroxene fabrics resulting from glide on (010), but (100) is generally found to be the most common glide plane in orthopyroxene naturally deformed under high-temperature, low-stress conditions (Mainprice & Nicholas, 1989). We suggest that this apparently atypical slip system may instead have been activated during deformation at relatively low temperatures, near the lower limit of crystal plasticity in orthopyroxene, or may be related to the kinking of the crystal lattice that we describe in orthopyroxene in the parent rock.

The observed clinopyroxene LPOs indicate that glide occurred on (010)[100], an atypical slip system in clinopyroxene. The most commonly reported slip system for clinopyroxene is (100)[001] (Kirby & Christie, 1977; Ave'Lallemant, 1978; Kollé & Blacic, 1983; Kirby & Kronenberg, 1984). Bascou *et al.* (2002) and Ulrich & Mainprice (2005) reported a similar slip system to those observed in this shear zone from naturally deformed eclogites, suggesting that (010)[100]-glide may be related to deformation under high confining pressures.

Flow stress estimates

Flow stresses can be estimated using recrystallized grain-size piezometers, but these are currently experimentally calibrated only for monophase aggregates, and thus can be applied only in the monophase olivine domain of the shear zone. Assuming that there has been no static grain growth following dynamic recrystallization in this material, the recrystallized grain-size paleopiezometric relationship of van der Wal *et al.* (1993) can be used to estimate that the grain sizes of $\bar{D} \sim 30$–100 μm developed at flow stresses of the order of 65–100 MPa. The microstructures that we observe in this domain indicate that a significant amount of recovery occurred, so there may have been some grain growth after deformation. Hence, this estimate of flow stresses is a minimum. This estimated flow stress is less than the peak strength of the upper mantle that is predicted if it is assumed that this strength is controlled by dislocation creep of olivine (Bürgmann & Dresen, 2008).

If we assume that olivine and orthopyroxene show the same bulk behaviour during grain-size-sensitive creep, we can also examine the evolution of flow stresses during deformation using a deformation mechanism map (Fig. 12). This analysis is subject to a number of assumptions. First, the deformation mechanism map is constructed for dry olivine. We assume that this map is applicable, as we infer that most water in the peridotite was bound in the structure of amphibole, which formed before initiation of the shear zone. Our geothermometric data indicate that the shear zone initiated at >750°C, and continued to operate to 650°C. We cannot accurately constrain the strain rate but it is likely that it was at the fast end of typical geological strain rates (Pfiffner & Ramsay, 1982) to cause the localization. Hence, we examine the case of a shear zone active at $\dot{\varepsilon} = 10^{-11}$ s^{-1}.

The presence of LPO and grain shape fabrics in the monophase domain indicate that shear zone initiation occurred in the dislocation creep regime. For a strain rate of $\dot{\varepsilon} = 10^{-11}$ s^{-1}, dislocation creep would have required flow stresses of the order of 0·8 GPa (at 'S', Fig. 12). If these high stresses were maintained throughout deformation, there would have been a rapid increase in strain rate (path 'A'; Fig. 12). Alternatively, constant strain rate deformation (path 'B'; Fig. 12) is consistent with a reduction in stress during development of a finer grain size, and a transition to dislocation-accommodated grain boundary sliding (disGBS; Hirth & Kohlstedt, 2003) and then grain-size-sensitive creep. We favour the latter interpretation because recrystallized grain-size piezometry indicates that a lower stress was experienced within the monophase domain. However, we note that both paths result in a decrease in $\sigma/\dot{\varepsilon}$, and thus would have resulted in strain-softening and localization (Hobbs *et al.*, 1990).

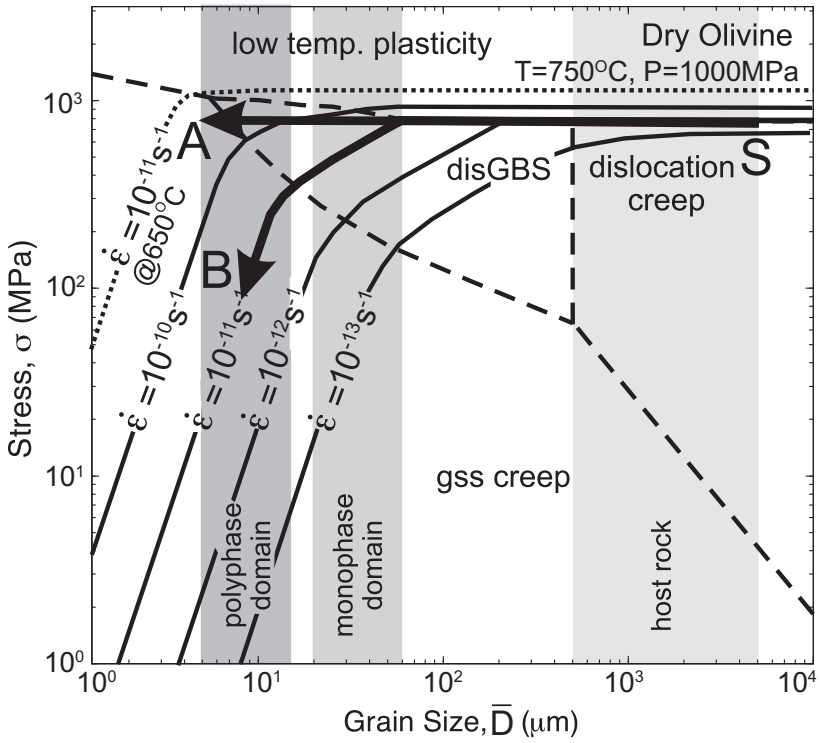

Fig. 12. Deformation mechanism map for dry olivine at 750°C, illustrating possible $\bar{D}$–σ paths during formation of, and deformation within, the shear zone. The deformation mechanism map uses constitutive equations described by Warren & Hirth (2006). Grain sizes measured in the various domains of the host-rock and shear zone are illustrated by grey rectangles. Possible $\bar{D}$–σ paths, indicated by bold black lines with arrowheads, are discussed further in the text. gss creep = grain-size-sensitive creep; disGBS = dislocation-accommodated grain boundary sliding.

Chemical reactions within the polyphase domain

The transition in deformation mechanisms from dislocation creep to grain-size-sensitive (diffusion) creep requires grain-size reduction. In these rocks, grain-size reduction was associated with reactions within the polyphase domain of the shear zone.

It has been shown that metamorphic equilibration proceeds most rapidly in deforming materials, as a result of increased surface area and internal strain energy (Stünitz & Tullis, 2001; de Ronde *et al.*, 2004; Holyoke & Tullis, 2006b). In our example, the observed difference in mineral chemistries between the host and the shear zone is probably due to retrograde reactions that continued at lower temperatures in the shear zone as compared with the host. Experimental investigation of the compositions of coexisting quadrilateral pyroxenes indicates that decreasing temperatures are consistent with an increase in the Ca-content and Mg/(Mg + Fe) in clinopyroxene and a decrease in the Ca-content and Mg/(Mg + Fe) in orthopyroxene (e.g. Lindsley, 1983). Thus, the differences in pyroxene compositions between the host-rock and shear zone indicate that the pyroxenes in the shear zone probably equilibrated at lower temperatures than those in the host-rock (Fig. 11a and b), an interpretation consistent with the results of two-pyroxene geothermometry (Table 2). We suggest that the deformation that was concentrated in the shear zone enhanced the kinetics of retrograde re-equilibration.

Given the low Cr content of the pyroxenes and olivine, Cr-depletion observed in finer spinel in the shear zone (Fig. 11c) must have been a dilution effect during production of greater volumes of this mineral. Aluminium is also required to create spinel, and this element may have been derived from breakdown of amphibole, reflected in a decrease in Al in fine-grained amphiboles over their parents (Fig. 11d; disregarding the small number of host amphiboles that were initially very Al-deficient). If so, amphibole production predated formation of fine pyroxenes + spinel. The pyroxenes were also probably involved in the retrograde reaction that modified the compositions of the spinels and amphiboles. This scenario makes a complete understanding of the microchemical evolution of this shear zone relatively complicated. Rather, we suspect that the reaction that induced chemical modification of the minerals in the fine-grained material continued after the these same reactions stopped operating in the host-rocks.

Causes of shear localization

Our results indicate that compositional variations are important for localizing strain in a variety of ways during deformation of peridotites in the lower lithosphere. We discuss these concepts further below.

Ductile shear instabilities in heterogeneous materials

A large advantage of our study is that we have the field context, and there are multiple field observations that are relevant to this issue. First, these ultramylonite zones are rare in the field area; this zone was the only one observed in the ~90 m^2 area we mapped. Second, folded orthopyroxenite dikes are also rare in this area; most orthopyroxenite dikes are planar. Third, the fold axial plane is everywhere consistently oriented ~162°/79°E, subparallel to a foliation (oriented ~159°/72°NE).

The shear zone developed approximately on a plane of maximum shear stress, as determined by the following analysis. Immediately adjacent to the shear zone, the orthopyroxenite dike is oriented approximately perpendicular to the lineation in the host-rock, assumed to be parallel to the long axis of the finite strain ellipsoid for the host-rock (X_H). This lineation is also parallel to the hinge line of folds of the orthopyroxenite dike. The orthopyroxenite dike thus intersects the shear zone approximately parallel to X_H, and the angular separation of the shear zone from the axial plane of the folded dike is 49° (Fig. 2e). The shear zone therefore lies approximately parallel to the expected orientation of a plane of maximum shear strain rate during the bulk strain that resulted in formation of the host-rock fabric. In the case of isotropic, viscous behaviour, this orientation is also the plane of maximum shear stress.

We suggest that the orthopyroxenite dike at this location was uniquely oriented so that a buckling instability did not initiate at this position during shortening. Instead, a ductile shear zone nucleated along a plane of maximum shear strain rate/shear stress. In this way, the presence of a rheological heterogeneity resulted in formation of a stress heterogeneity, which inherently led to a variation in strain rate. Similar effects are denoted on a variety of crustal levels (e.g. Goodwin & Tikoff, 2002), such as the nucleation of shear zones on the margins of basaltic dikes in granitic crustal rocks (e.g. Sengupta, 1997).

Microstructural processes that promoted a deformation mechanism transition

Our microstructural and textural data indicate that, following initiation of the shear zone, pyroxene grains derived from the two dikes were entrained with host-rock olivine and minor pyroxenes during shearing. All phases experienced grain-size reduction that promoted a transition from dislocation creep to grain-size-sensitive creep. Grain-size-sensitive creep operates at a lower ratio of $\sigma/\dot{\varepsilon}$ than dislocation creep under equivalent conditions (e.g. Fig. 12), so this transition would have resulted in localization.

The mechanism by which phase mixing and grain-size reduction occurred is not entirely clear. Orthopyroxene and clinopyroxene within the polyphase domain of the shear zone have LPOs consistent with dislocation creep. Smaller, high-Schmid factor orthopyroxene grains, such as those illustrated in Fig. 8b, most probably formed by dynamic recrystallization of the orthopyroxene porphyroclasts along their margins. With increasing distance from the porphyroclasts, the proportion of pyroxene decreases (e.g. Fig. 7), suggesting that the newly formed pyroxene grains were mixed with olivine by grain boundary sliding during deformation. It is likely that olivines and both pyroxenes experienced initial grain-size reduction by dynamic recrystallization accommodated by dislocation creep.

However, this process alone cannot result in sufficient grain-size reduction to maintain a deformation mechanism switch to grain-size-sensitive creep in a monophase material (de Bresser *et al.*, 1998, 2001). On the other hand, in polyphase aggregates, grain growth may be inhibited by pinning of grain boundaries (e.g. Herwegh & Kunze, 2002). We suggest that small grain sizes were retained in the polyphase domain, following grain-size reduction by dislocation creep, because the shear zone contains a mixture of olivine and pyroxene.

Reactions that promoted a deformation mechanism transition

Amphibole is present in both the host-rock and the shear zone. In general, amphibole-rich areas in the host-rock are not particularly fine-grained, and have not become aligned in through-going zones. We therefore consider it unlikely that the amphibole-producing reaction alone was responsible for the grain-size reduction necessary to promote a transition to grain-size-sensitive creep in a coarse-grained starting aggregate.

On the other hand, the chemical compositions of the fine-grained material that makes up much of the shear zone proper are distinct from that of the host. The reactions that produced this fine-grained material may, for the most part, be continuous (see Newman *et al.*, 1999). In the less deformed host-rock, these continuous reactions could be accommodated by cation diffusion and the nucleation of new grains might not have been necessary. However, we suggest that the strain energy resulting from the earlier stages of deformation within the shear zone promoted the nucleation of fine-grained mixtures of minerals with compositions that are distinct from those of pre-existing grains (see Newman *et al.*, 1999). Reaction rates would also have been enhanced by the small grain size resulting from dynamic recrystallization. It is likely that formation of these reaction products did contribute to the grain-size

reduction that promoted the deformation mechanism switch to grain-size-sensitive creep.

Strain localization: strain-softening vs strain-hardening material

During grain-size-sensitive creep, grain growth in the polyphase parts of the ultramafic ultramylonitic shear zone was prohibited by the presence of additional phases (pyroxenes and amphiboles), so the grain size remained small enough for grain-size-sensitive deformation mechanisms to dominate. As illustrated in Fig. 12, grain-size-sensitive mechanisms require lower ratios of $\sigma/\dot{\varepsilon}$ than dislocation creep under the same conditions; hence this deformation mechanism switch resulted in shear localization.

The critical field observation, however, is that the shear zone does not extend far beyond the location of the pyroxenite dikes. Thus, despite high shear strain values recorded in the shear zone, there is no outward propagation of the shear zone in the absence of the pyroxene. This observation suggests that the surrounding monophase domain did not experience strain softening via a deformation mechanism switch, despite a significant reduction in grain size. In fact, the lack of outward propagation of the shear zone suggests that the lithospheric mantle, at the conditions of deformation recorded by this ultramylonite zone, does not experience strain softening. This observation is consistent with the arguments of Hobbs *et al.* (1990) and, in fact, is a compelling field example of their hypothesis that many zones that show localization are, in fact, strain hardening.

CONCLUSIONS

To conclude, our data suggest that the ultramafic ultramylonitic shear zone initially nucleated as a result of a strain rate/stress heterogeneity resulting from a rheological heterogeneity between the orthopyroxenite dike and the surrounding peridotite mass during bulk shortening. During this event, a zone of moderately fine-grained olivine with some intermixed pyroxene and amphibole was formed. The microstructures and LPO data indicate that initial grain-size reduction of olivine and orthopyroxene primarily occurred by dynamic recrystallization accommodated by dislocation creep. During this deformation, pyroxene and amphibole from adjacent pyroxenite dikes and host-rocks were entrained in the shear zone, resulting in some phase mixing. Deformation resulted in enhanced reaction kinetics in layers within the shear zone that were polyphase. The aggregates developed within the shear zone were fine-grained and intermixed, inhibiting grain growth, resulting in a switch in the dominant deformation mechanism from dislocation creep to grain-size-sensitive (diffusion) creep in polyphase domains of the shear zone.

Deformation was focused into this weaker material, resulting in a shear instability. However, the surrounding monophase domain did not experience strain softening via a deformation mechanism switch. The presence of the surrounding monophase host-rocks therefore prevented the shear zone in the polyphase domain from propagating further. These observations support theoretical predictions that a deformation mechanism switch is unlikely to occur in monophase materials, as proposed by de Bresser *et al.* (1998, 2001), and indicates the importance of compositional heterogeneity to stress localization in the mantle.

ACKNOWLEDGEMENTS

We are grateful for scientific discussions and technical advice offered by C. Holyoke and G. Medaris, and technical assistance of J. Fournelle, T. Stephens and R. Guillemette during SEM and microprobe work. We thank J. Warren for the Matlab script, from which Fig. 12 was constructed. Reviews by D. Prior and P. Skemer resulted in significant improvements to the manuscript.

FUNDING

This work was supported by funding from the Packard Foundation to B.T., and the American National Science Foundation (grant number EAR 0409522) to B.T. and J.N. The FE-SEM acquisition at Texas A&M University was supported by the American National Science Foundation (grant number DBI-0016835), the Vice President for Research Office at Texas A&M University, and the Texas Engineering Experimental Station.

SUPPLEMENTARY DATA

Supplementary data for this paper are available at *Journal of Petrology* online.

REFERENCES

Ave'Lallemant, H. G. (1967). Structural and petrological analysis of an 'Alpine-type' peridotite. The lherzolite of the French Pyrenees. *Leidse Geologische Mededelingen* **42**, 1–57.

Ave'Lallemant, H. G. (1978). Experimental deformation of diopside and websterite. *Tectonophysics* **48**, 1–27.

Ave'Lallemant, H. G. & Carter, N. L. (1970). Syntectonic recrystallization of olivine and modes of flow in the upper mantle. *Geological Society of America Bulletin* **81**, 2203–2220.

Bai, Q. & Kohlstedt, D. L. (1992). High-temperature creep of olivine single crystals; 2, Dislocation structures. *Tectonophysics* **206**, 1–29.

Bai, Q., Mackwell, S. J. & Kohlstedt, D. L. (1991). High-temperature creep of olivine single crystals 1. Mechanical results for buffered samples. *Journal of Geophysical Research* **96**, 2441–2463.

Ballhaus, C., Berry, R. F. & Green, D. H. (1991). High pressure experimental calibration of the olivine–orthopyroxene–spinel oxygen geobarometer: implications for the oxidation state of the upper mantle. *Contributions to Mineralogy and Petrology* **107**(1), 27–40.

Bascou, J., Tommasi, A. & Mainprice, D. (2002). Plastic deformation and development of clinopyroxene lattice-preferred orientation in eclogites. *Journal of Structural Geology* **24**, 1357–1368.

Ben Ismaïl, W. & Mainprice, D. (1998). An olivine fabric database: an overview of upper mantle fabrics and seismic anisotropy. *Tectonophysics* **296**, 145–157.

Bestmann, M. & Prior, D. J. (2003). Intragranular dynamic recrystallization in naturally deformed calcite marble: diffusion accommodated grain boundary sliding as a result of subgrain rotation recrystallization. *Journal of Structural Geology* **25**(10), 1597–1613.

Boudier, F. & Coleman, R. G. (1981). Cross section through the peridotite in the Samail ophiolite, southeastern Oman Mountains. *Journal of Geophysical Research* **86**, 2573–2592.

Boullier, A. M. (1986). Sense of shear and displacement estimates in the Abeibara–Rarhous late Pan-African shear zone, Adrar des Iforas, Mali. *Journal of Structural Geology* **8**, 47–58.

Brace, W. F. & Kohlstedt, D. L. (1980). Limits on lithospheric stress imposed by laboratory experiments. *Journal of Geophysical Research* **85**(B11), 6248–6252.

Bürgmann, R. & Dresen, G. (2008). Rheology of the lower crust and upper mantle: Evidence from rock mechanics, geodesy, and field observations. *Annual Review of Earth and Planetary Sciences* **36**, 531–567.

Carter, N. L. & Ave'Lallemant, H. G. (1970). High temperature flow of dunite and peridotite. *Geological Society of America Bulletin* **81**, 2181–2202.

Carter, N. L., Barker, D. W. & George, R. P., Jr (1972). Seismic anisotropy flow, and constitution of the upper mantle. In: Heard, H. C., Borg, I. Y., Carter, N. L. & Rayleigh, C. B. (eds) *Flow and Fracture of Rocks*. AGU Geophysical Monograph **16**, Washington, DC: American Geophysical Union167–190.

Christensen, N. I. & Lundquist, S. M. (1982). Pyroxene orientation in the upper mantle. *Geological Society of America Bulletin* **93**, 279–288.

de Bresser, J. H. P., Peach, C. J., Reijs, J. P. J. & Speirs, C. J. (1998). On dynamic recrystallization during solid state flow: effects of stress and temperature. *Geophysical Research Letters* **25**, 3457–3460.

de Bresser, J. H. P., Ter Heege, J. H. & Spiers, C. J. (2001). Grain size reduction by dynamic recrystallization: can it result in major rheological weakening? *International Journal of Earth Sciences (Geologische Rundschau)* **90**, 28–45.

de Ronde, A. A., Heilbronner, R., Stünitz, H. & Tullis, J. (2004). Spatial correlation of deformation and mineral reaction in experimentally deformed plagioclase–olivine aggregates. *Tectonophysics* **389**, 93–109.

Dijkstra, A. H., Drury, M. & Vissers, R. L. M. (2001). Structural petrology of plagioclase peridotites in the West Othris Mountains (Greece): Melt impregnation in mantle lithosphere. *Journal of Petrology* **42**(1), 5–24.

Dijkstra, A. H., Drury, M. & Frijhoff, R. M. (2002). Microstructures and lattice fabrics in the Hilti mantle section (Oman Ophiolite): Evidence for shear localization and melt weakening in the crust–mantle transition zone? *Journal of Geophysical Research* **107**(B11), 2270.

Etheridge, M. A. (1975). Deformation and recrystallisation of orthopyroxene from the Giles Complex, central Australia. *Tectonophysics* **25**, 87–114.

Etheridge, M. A. & Hobbs, B. E. (1974). Chemical and deformation controls on recrystallization of mica. *Contributions to Mineralogy and Petrology* **43**, 111–124.

Exner, M. E. (1972). Analysis of grain and particle size distribution in metallic materials. *International Metallurgical Reviews* **17**, 25–82.

Ferre, E. C., Tikoff, B. & Jackson, M. (2005). The magnetic anisotropy of mantle peridotites: Example from the Twin Sisters dunite, Washington. *Tectonophysics* **398**, 141–166.

Fitz Gerald, J. D. & Stünitz, H. (1993). Deformation of granitoids at low metamorphic grade I; Reactions and grain size reduction. *Tectonophysics* **221**, 269–297.

Fliervoet, T. F., Drury, M. R. & Chopra, P. N. (1999). Crystallographic preferred orientations and misorientations in some olivine rocks deformed by diffusion or dislocation creep. *Tectonophysics* **303**, 1–27.

Fliervoet, T. F., White, S. H. & Drury, M. R. (1997). Evidence for dominant grain-boundary sliding deformation in greenschist- and amphibolite grade polymineralic ultramylonites from the Redbank deformed zone, central Australia. *Journal of Structural Geology* **19**, 1495–1520.

Furusho, M. & Kanagawa, K. (1999). Transformation-induced strain localization in a lherzolite mylonite from the Hidaka metamorphic belt of central Hokkaido, Japan. *Tectonophysics* **30**, 411–432.

Gasparik, T. (1987). Orthopyroxene thermobarometry in simple and complex systems. *Contributions to Mineralogy and Petrology* **96**, 357–370.

Gilotti, J. A. & Hull, J. M. (1990). Phenomenological superplasticity in rocks. In: Knipe, R. J. & Rutter, E. H. (eds) *Deformation Mechanisms, Rheology and Tectonics. Geological Society, London, Special Publications* **54**, 229–240.

Goetze, C. & Evans, B. (1979). Stress and temperature in the bending lithosphere as constrained by experimental rock mechanics. *Geophysical Journal of the Royal Astronomical Society* **59**, 463–478.

Goodwin, L. B. & Tikoff, B. (2002). Competency contrast, kinematics, and the development of foliations and lineations in the crust. *Journal of Structural Geology* **24**, 1065–1085.

Gueguen, Y. & Nicolas, A. (1980). Deformation of mantle rocks. *Annual Review of Earth and Planetary Sciences* **8**, 119–144.

Handy, M. R. (1990). The solid-state flow of polymineralic rocks. *Journal of Geophysical Research* **96**(B6), 8647–8661.

Handy, M. R. (1994). Flow laws for rocks containing two non-linear viscous phases: a phenomenological approach. *Journal of Structural Geology* **16**(3), 287–301.

Handy, M. R., Wissing, S. B. & Streit, L. E. (1999). Frictional–viscous flow in mylonite with varied bimineralic composition and its effect on lithospheric strength. *Tectonophysics* **303**, 175–191.

Helmstaedt, H., Anderson, O. L. & Gavasci, A. T. (1972). Petrofabric studies of eclogite, spinel-websterite, and spinel-lherzolite xenoliths from kimberlite-bearing breccia pipes in southeastern Utah and northeastern Arizona. *Journal of Geophysical Research* **77**, 4350–4365.

Herwegh, M. & Kunze, K. (2002). The influence of nano-scale second-phase particles on deformation in fine-grained calcite mylonites. *Journal of Structural Geology* **24**, 1463–1478.

Hirth, G. & Kohlstedt, D. (2003). Rheology of the upper mantle and the mantle wedge: a view from the experimentalists. In: Eiler, J. (ed.) *Inside the Subduction Factory. American Geophysical Union, Geophysical Monographs* **138**, 83–105.

Hobbs, B. E., Mühlhaus, H.-B. & Ord, A. (1990). Instability, softening, and localization of deformation. In: Knipe, R. J. & Rutter, E. H. (eds) *Deformation Mechanisms, Rheology and Tectonics. Geological Society, London, Special Publications* **54**, 143–165.

Holtzman, B. K., Kohlstedt, D. L., Zimmerman, M. E., Heidelbach, F., Hiraga, T. & Hustoft, J. (2003). Melt segregation and strain partitioning: Implications for seismic anisotropy and mantle flow. *Science* **301**, 1227–1230.

Holyoke, C. W. & Tullis, J. (2006*a*). Formation and maintenance of shear zones. *Geology* **34**(2), 105–108.

Holyoke, C. W. & Tullis, J. (2006*b*). The interaction between reaction and deformation: an experimental study using a biotite + plagioclase + quartz gneiss. *Journal of Metamorphic Geology* **24**, 743–762.

Imber, J., Holdsworth, R. E., Butler, R. & Strachan, R. A. (2001). A reappraisal of the Sibson–Scholz fault zone model: The nature of the frictional to viscous ('brittle–ductile') transition along a

long-lived, crustal-scale fault, Outer Hebrides, Scotland. *Tectonics* **20**(5), 601–624.

Jackson, E. D. (1961). Primary textures and mineral associations in the ultramafic zone of the Stillwater complex, Montana. *US Geological Survey, Professional Papers* **358**.

Ji, S. & Zhao, P. (1993). Flow laws of multiphase rocks calculated form experimental data on the constituent phases. *Earth and Planetary Science Letters* **117**, 181–187.

Ji, S., Wang, Q., Xia, B. & Marcotte, D. (2004). Mechanical properties of multiphase materials and rocks: a phenomenological approach using generalized means. *Journal of Structural Geology* **26**, 1377–1390.

Jin, D., Karato, S.-I. & Obata, M. (1998). Mechanisms of shear localization in the continental lithosphere: inference from the deformation microstructures of peridotites in the Ivrea zone, northwestern Italy. *Journal of Structural Geology* **20**(2–3), 195–209.

Jung, H. & Karato, S.-I. (2001). Water-induced fabric transitions in olivine. *Science* **293**, 1460–1462.

Kirby, S. H. (1983). Rheology of the lithosphere. *Reviews of Geophysics and Space Physics* **21**, 1458–1487.

Kirby, S. H. & Christie, J. M. (1977). Mechanical twinning in diopside $Ca(Mg,Fe)Si_2O_6$; structural mechanism and associated crystal defects. *Physics and Chemistry of Minerals* **1**(2), 137–163.

Kirby, S. H. & Kronenberg, A. K. (1984). Deformation of clinopyroxenite: evidence for a transition in flow mechanisms and semibrittle behaviour. *Journal of Geophysical Research* **89**(B3), 2381–2393.

Kohlstedt, D. L. (1976). New technique for decorating dislocations in olivine. *Science* **191**, 1045–1046.

Kohlstedt, D. L. & Goetze, C. (1974). Low-stress high-temperature creep in olivine single crystals. *Journal of Geophysical Research* **79**, 2045–2051.

Kollé, J. J. & Blacic, J. D. (1983). Deformation of single-crystal clinopyroxenes; 2. Dislocation-controlled flow processes in hedenbergite. *Journal of Geophysical Research* **89**(B5), 3177–3192.

Kruckenberg, S. Tikoff, B., Young, L. I. & Newman, J. (2008). Relationships between compositional layering, structural fabric, and the formation of melt pathways in the Twin Sisters complex, Washington State. Abstract and Poster. *AGU Chapman Conference on Shallow Mantle Composition and Dynamics/Fifth International Orogenic Lherzolite Conference, Mt. Shasta, California, 22–26 September 2008.*

Lacassin, R., Leloup, P. H. & Tapponnier, P. (1993). Bounds on strain in large Tertiary shear zones of SE Asia from boudinage restoration. *Journal of Structural Geology* **15**, 677–692.

Lamb, W. M. & Popp, R. K. (2009). Amphibole equilibria in mantle rocks: Determining values of mantle a_{H2O} and implications for mantle H_2O contents. *American Mineralogist* **94**, 41–52.

Lindsley, D. H. (1983). Pyroxene thermometry. *American Mineralogist* **68**, 477–493.

Mainprice, D. & Nicholas, A. (1989). Development of shape and lattice-preferred orientations: application to seismic anisotropy of the lower crust. *Journal of Structural Geology* **11**(1–2), 175–189.

Mercier, J.-C. C. (1985). Olivine and pyroxenes. In: Wenk, H. R. (ed.) *Preferred Orientation in Deformed Metals and Rocks: An Introduction to Modern Texture Analysis*. Orlando, FL: Academic Press, pp. 407–430.

Naze, L., Doukhan, J. C. & Latrons, K. (1987). A TEM study of lattice defects in naturally and experimentally deformed orthopyroxenes. *Bulletin de Minéralogie* **110**, 497–512.

Newman, J., Lamb, W. M., Drury, M. R. & Vissers, R. L. M. (1999). Deformation processes in a peridotite shear zone: reaction-softening by an H_2O-deficient continuous net transfer reaction. *Tectonophysics* **303**, 193–222.

Nicolas, A. & Poirier, J. P. (1976). *Crystalline Plasticity and Solid State Flow in Metamorphic Rocks*. London: John Wiley.

Norris, R. J. & Cooper, A. F. (2003). Very high strains recorded in mylonites along the Alpine Fault, New Zealand: implications for the deep structure of plate boundary faults. *Journal of Structural Geology* **25**, 2141–2157.

Onyeagoucha, A. C. (1978). Twin Sisters dunite: petrology and mineral chemistry. *Geological Society of America Bulletin* **89**, 1459–1474.

Pfiffner, O. A. & Ramsay, J. G. (1982). Constraints on geological strain rates; arguments from strain states of naturally deformed rocks. *Journal of Geophysical Research* **87**(B1), 311–321.

Poirier, J. P. & Guillopé, M. (1979). Deformation-induced recrystallisation in minerals. *Bulletin de Minéralogie* **102**, 67–74.

Popp, R. K., Virgo, D., Yoder, H. S., Hoering, T. C. & Phillips, M. W. (1995). An experimental study of phase equilibria and Fe oxy-component in kaersutitic amphibole: Implications for the fH_2O and a_{H2O} in the upper mantle. *American Mineralogist* **80**, 534–548.

Prior, D. J., Boyle, A. P., Brenker, F., Cheadle, M. C., Day, A., Lopez, G., Purezzo, L., Potts, G. J., Reddy, S., Spiess, R., Timms, N. E., Trimby, P. W., Wheeler, J. & Zetterstrom, L. (1999). The application of electron backscatter diffraction and orientation contrast imaging in the SEM to textural problems in rocks. *American Mineralogist* **84**, 1741–1759.

Raj, J. & Ashby, M. F. (1971). On grain boundary sliding and diffusional creep. *Metallurgical and Materials Transactions B* **2**, 1113–1127.

Ranalli, G. & Murphy, D. C. (1987). Rheological stratification of the lithosphere. *Tectonophysics* **132**, 281–296.

Rutter, E. H. & Brodie, K. H. (1988). The role of tectonic grain size reduction in the rheologic stratification of the lithosphere. *Geologische Rundschau* **77**(1), 295–308.

Sengupta, S. (1997). Contrasting fabrics in deformed dikes and host rocks: natural examples and a simplified model. In: Sengupta, S. (ed.) *Evolution of Geological Structures in Micro- to Macro-scales*. London: Chapman and Hall, pp. 341–372.

Skemer, P. & Karato, S.-I. (2008). Sheared lherzolite xenoliths revisited. *Journal of Geophysical Research* **113**, doi:10/1029.2007JB005286.

Skemer, P., Katayaman, I. & Karato, S.-I. (2006). Deformation fabrics of the Cima di Gragnone peridotite massif, Central Alps, Switzerland: evidence for deformation at low temperatures in the presence of water. *Contributions to Mineralogy and Petrology* **152**, 43–51.

Strotzki, W., Wedel, A., Weber, K. & Muller, W. F. (1990). Microstructure and texture in lherzolites of the Balmuccia massif and their significance regarding the thermomechanical history. *Tectonophysics* **179**, 227–251.

Stünitz, H. & Fitz Gerald, J. D. (1993). Deformation of granitoids at low metamorphic grade II; Granular flow in albite-rich mylonites. *Tectonophysics* **221**, 299–324.

Stünitz, H. & Tullis, J. (2001). Weakening and strain localization produced by syn-deformation reaction of plagioclase. *Tectonophysics* **90**, 136–148.

Sundberg, M. & Cooper, R. F. (2008). Crystallographic preferred orientation produced by diffusional creep of harzburgite: The effects of chemical interactions amongst phases during plastic flow. *Journal of Geophysical Research* **113**(B12208), doi:10.1029/2008JB005618.

Taylor, W. R. (1998). An experimental test of some geothermometer and geobarometer formulations for upper mantle peridotites with application to the thermobarometry of fertile lherzolite and garnet websterite. *Neues Jahrbuch für Mineralogie* **178**, 381–408.

Toy, V. G., Norris, R. J. & Prior, D. J. (2008). Quartz fabrics in the Alpine Fault mylonites: Influence of pre-existing preferred orientations on fabric development during progressive uplift. *Journal of Structural Geology* **30**, 602–621.

Treagus, S. H. & Sokoutis, D. (1992). Laboratory modeling of strain variation across rheological boundaries. *Journal of Structural Geology* **14**, 405–424.

Tullis, J. & Yund, R. A. (1987). Transition from cataclastic flow to dislocation creep of feldspar: Mechanisms and microstructures. *Geology* **15**, 606–609.

Tullis, T. E., Horowitz, F. G. & Tullis, J. (1991). Flow laws of polyphase aggregates from end-member flow laws. *Journal of Geophysical Research* **96**, 8081–8096.

Twiss, R. J. (1976). Structural superplastic creep and linear viscosity in the Earth's mantle. *Earth and Planetary Science Letters* **33**, 86–100.

Ulrich, S. & Mainprice, D. (2005). Does cation ordering in omphacite influence development of lattice-preferred orientation? *Journal of Structural Geology* **27**, 419–431.

van der Wal, D. & Vissers, R. L. M. (1993). Uplift and emplacement of upper mantle rocks in the western Mediterranean. *Geology* **21**, 1119–1122.

van der Wal, D., Chopra, P., Drury, M. & Fitz Gerald, J. (1993). Relationships between dynamically recrystallized grain size and deformation conditions in experimentally deformed olivine rocks. *Geophysical Research Letters* **20**(14), 1479–1482.

Vissers, R. L. M., Drury, M. R., Hoogerduijn Strating, E. H., Spiers, C. J. & van der Wal, D. (1995). Mantle shear zones and their effect on lithospheric strength during continental breakup. *Tectonophysics* **249**, 155–171.

Warren, J. M. & Hirth, G. (2006). Grain size sensitive deformation mechanisms in naturally deformed peridotites. *Earth and Planetary Science Letters* **248**, 438–450.

Webber, C. W., Little, T., Newman, J. & Tikoff, B. (2008). Fabric superposition in upper mantle peridotite, Red Hills, New Zealand. *Journal of Structural Geology* **30**, 1412–1428.

Wheeler, J. (1992). Importance of pressure solution and coble creep in the deformation of polymineralic rocks. *Journal of Geophysical Research* **97**, 4579–4586.